Cs, Ba, Co, and Eu sorption on biotite at pH 5-9 and at varying ionic strength

Pawan Kumar*, Stellan Holgersson and Christian Ekberg
Department of Chemistry and Chemical Engineering, Division of Nuclear Chemistry
Chalmers University of Technology, Kemivägen 4, SE-41296 Göteborg, Sweden

Abstract

The sorption of ^{134}Cs, ^{133}Ba, ^{60}Co and ^{152}Eu on biotite mineral at pH 5-9 and room temperature with pH buffered solutions of 0.001-0.1 M $NaClO_4$ was investigated. Experimental data was collected for biotite suspensions by batch sorption of radionuclides, potentiometric titrations, tritium exchange and cation exchange capacity experiments. The results were modelled with one amphoteric (2-pKa) surface complexation site and one cation exchange site. The batch sorption of tracer concentration [10^{-8}M] radionuclides onto crushed biotite of size fraction 0.250-0.500 mm with S: L = 1:50 was studied at three different ionic strengths of $NaClO_4$ solutions and at five different pH (5,6,7,8,9) at room temperature (~25 °C) for up to two months in anoxic ([O_2]<1ppm) atmosphere. The measured sorption coefficient (R_d) was found to increase with time continuously up to about 1 month.

For I= 0.001 M and the pH range 5-9, the results at 2 months gave Rd = 0.6-1.2, 0.3-8.3, 0.01-1.9 and 2.7-18 m^3/kg for Cs, Ba, Co and Eu, respectively. For I=0.01 M, the corresponding results were R_d = 0.1-0.7, 0.01-4.4, 0.01-7.5 and 0.2-4.3 m^3/kg and for I= 0.1 M, R_d = 0.01-0.2, 0.03-0.4, 0.01-4.7 and 2.1-6.7 m^3/kg. It was found that pH influenced the sorption since clear sorption "edges" were established for all the radionuclides at about pH 7. In the case of Co and Eu, sorption decreased at higher pH values. Increasing ionic strength suppressed sorption of Cs and Ba but had less influence on the sorption of Co and Eu.

Titrations on solid phase suspensions were made from pH ~3 to 11 and from these two pKa values (-4.9 and -7.1) were modelled for the biotite surface. Modelling of titration data was made by coupling PHREEQC chemical speciation calculations with an error minimization routine. The specific surface area with BET model, site density and cation exchange capacity of the same biotite size fraction were determined separately and gave the values 0.47±0.01 m^2/g, 3.18±0.66·10^{-6} mol/g and 1.01±0.03·10^{-2} cmolc/kg, respectively. Modelling of the sorption was made to fit the final sorption experimental data at 2 months, with compensation for biotite dissolution. This was accomplished with the use of PHREEQC software coupled with an optimization routine written in PYTHON programming language. Sorption of all four elements was successfully modelled with a combination of one acidic/amphoteric 2-pKa surface complexation site and one ion exchange site. The model did not include any compensation for surface electrostatic effects.

Keywords: biotite, radionuclides, sorption, surface complex, ion exchange, modelling

1. Introduction

In 2023, in Sweden, about 40% of the electricity was produced by the means of nuclear power. For 2050, the domestic demand for electricity is predicted to double or treble due to the phasing out of fossil fuels. In Sweden today the fossil fuels are mainly used in the steel industry and the transport sector but not for electricity production. To have nuclear power as part of a sustainable energy mix in the future, the problem with High-Level radioactive Waste (HLW) in the form of spent nuclear fuel must be solved. This task has now been accomplished in both Sweden and Finland by the on-going or planned building of deep geological repositories in formations of granitic rock according to the KBS-3 concept [1], [2], [3] that will store the spent fuel safely for up to 10^5 years.

In Sweden, the SKB company has the responsibility to construct and operate a deep geological nuclear waste repository planned to be built located near the Forsmark NPP, situated in the municipality of Östhammar, about 150km north of Stockholm. After extensive geological investigations this site was found to be the best site for a geological disposal of spent nuclear fuel storage of those investigated [3]. The KBS-3 concept is a multibarrier design comprising of spent fuel placed in steel inserts in welded copper canisters. These are in turn to be placed into drilled holes in a granitic host rock at 500m depth, with a back-fill of bentonite clay. Around 12,000 tons of spent nuclear fuel is predicted to be generated from the currently running Swedish nuclear facilities, which corresponds to around 6000 spent fuel canisters to be placed inside the repository (ibid.).

In such scenarios where there is a breach in the copper canister, groundwater will be in contact with spent fuel and dissolve and the dissolved component will start to migrate through the bentonite. The surrounding host rock is then the last barrier that can prevent further radionuclide migration to the biosphere [4], [5]. Therefore, from a repository performance aspect, it is necessary to also understand the radionuclide retention properties of the bedrock matrix itself.

Both SKB and the Finnish company POSIVA have extensively studied the radionuclide sorption onto granitic rock. The results are mainly reported in the form of radionuclide distribution coefficients, K_d values [6], [7].

However, there are very few studies available that have modelled these condition-dependent empirical K_d with condition-independent chemical reaction models (Surface Complexation Models, SCM) for achieving an understanding of the underlying sorption mechanisms. Furthermore, such models have wider applicability since they can model for example the impact of groundwater composition on sorption. However, SCM can only be directly applied on pure phases, hence single minerals have to be studied one at a time, therefore the individual mineral SCM must be combined into an overall model, like the Component Additive approach [8], [9] of the complex solid phase of rock.

The rock type at the Forsmark site is a granodiorite and it is mainly composed of various feldspars, such as K-feldspar and plagioclase, along with minor components of mica minerals,

for example biotite and chlorite. In addition, in conductive fractures there are secondary minerals like calcite and clays to be found, mainly as fracture filling materials [10], [11].

The present work is intended to be the first in a series of studies of radionuclide sorption on single granitic minerals relevant for the Forsmark granodiorite, with systematic variation of pH and ionic strength. Due to its alleged importance for radionuclide sorption, biotite was selected as the first mineral to be studied.

Biotite belongs to the mica mineral family or sub-group of the phyllosilicate group. Like all phyllosilicates, biotite has a layered structure of tetrahedral layers of Si^{4+}, which are tetrahedrally coordinated to oxygen or hydroxyl groups and octahedral layers of divalent cations, preferentially Fe^{2+} and Mg^{2+}. Micas follow a tetrahedral-octahedral-tetrahedral (TOT) + cation structural pattern. Partial substitution of Si^{4+} with Al^{3+} in tetrahedral layers creates an overall negative charge of one TOT layer where the interlayer cations of non-hydrated K^+ bind the TOT layers together. These ions can be exchanged with other, less strongly bound, hydrated cations, which initiates a mineral dissolution process [12].

According to literature, biotite is considered to have a strong sorption capacity for radioactive elements [13], [14], [15], [16], [17]. Based on the layered structure of biotite, cations can be presumed to sorb either by ion-exchange, primarily on the basal planes, or by surface complexation on the edge sites. In the literature, several types of edge sites are presumed to exist, namely acidic(1-pKa) and/or amphoteric (2-pKa) sites of terminal hydroxyl groups of the silianol and aluminol types, respectively [18]. Furthermore, “activated” edge sites have been stipulated to occur in weathered biotite, so called Frayed Edge Sites (FES). The activation process is presumed to take place when hydrated ions have replaced interlayer K^+ in the nearby interlayer [13]. It is not entirely clear if FES themselves is responsible for increased cation uptake or if they just promote further in-diffusion of cations into the interlayer or if they do both [19]. In some modelling studies the hydroxyl edge sites have instead been considered as ion exchange sites [20], [17], [21].

In a recent literature review for SCM data for biotite, among other minerals, by [22] it was observed that the most implemented experimental method is the sorption isotherm, where pH is fixed and the concentration of sorbing element is varied. This type of study usually involves relatively high concentrations of the sorbing element. However, for a SCM implementation on experimental data, it is advisable to stay well below tracer concentration (10^{-6} M, according to the IUPAC definition) so that surface properties are not modified by the adsorption. Instead, for SCM studies a wide variation of the solution conditions like pH, ionic strength and temperature is more preferrable to obtain a robust model [23]

Furthermore, datasets with systematic variations of solution conditions were found to be rather lacking [22]. One study with pH variation at fixed ionic strength were found for the anionic Se(IV) where three surface complexation sites were utilized, all of the edge type [24]. Another study had pH fixed and varied ionic strength for alkaline earth cations, which was modelled with three cation exchange sites [21]. Only two studies were found where both pH and ionic strength were varied, both were studies on Eu(III) sorption onto biotite and these were modelled either by one surface complexation site and one ion exchange site [25] or with just one ion

exchange site [15]. To conclude, the different SCM for biotite that have been reported can hardly be said to be consistent. This is an unfortunate situation, especially if one would like to have a robust sorption model that can be used for a wide set of water conditions.

The aims of this investigation are therefore: 1) To characterize biotite with respect to specific surface area, cation exchange capacity, acidic site density and surface acidity in separate experiments, 2) To perform the sorption experiments with biotite and some representative elements and oxidation states, in this case Cs, Ba, Co, and Eu at well below tracer concentrations (10^{-8}M), with systematic variation of pH (5-9) and ionic strength (0.001,0.01 and 0.1 M) at room temperatures, and. 3) To model the measured R_d values with SCM, utilizing the PHREEQC geochemical modeling software coupled with a PYTHON programming optimization routine for obtaining the SCM constants.

A further aim is that this work may serve as a primer for future sorption studies of other minerals that constitute the Forsmark granodiorite. When several mineral datasets have been collected, a modelling of the R_d values for Forsmark granodiorite may be feasible using methods like the Component Addition approach.

2. Material and methods

2.1 Biotite sample preparation and measurement of its specific surface area

The biotite specimen used in this study originated from Risör, Norway. The composition has been determined to be $K_{1.05}(Mg_{0.70}Mn_{0.06}Ti_{0.18}Fe\ (II)_{1.81}Fe\ (III)_{0.25})\ Al_{1.28}Si_{2.62}O_{10}(OH)_2$ and, in the same study, the purity of the biotite specimen was estimated to be more than 99% [26]. Its density has previously been determined to 3.10kg/m^3 [27].

The mineral was found to be difficult to crush with mortar and pestle, therefore, the crushing was made with a blender machine equipped with steel blades (M20, IKA). The crushed mineral was then sieved by the use of stainless test sieves (200mm ISO3310-1 type, Retsch) and a sieve shaker machine (AS200, Retsch) into two particle size fractions: one 0.25-0.5mm fraction mainly for batch sorption, and one 0.063-0.125mm fraction for use in acidic density measurements only. The sieving was accomplished through a high amplitude shaking for 20-30 min., followed by a lower amplitude shaking for 1 h. The ultrafine particles were removed by washing with numerous portions of 95% ethanol. The clarity of the ethanol supernatant after settling of the coarse particles was taken as proof for ultrafine particle removal. The biotite was dried in a vacuum chamber for several days and then triplicate samples were taken for specific surface area (SSA) measurements. The SSA for both size fractions was determined with a Kr gas-adsorption instrument (ASAP2020, Micromeritics) and data evaluated with the BET-isotherm [28], utilizing the instrument software.

2.2 Measurement of cation exchange capacity (CEC)

The cation exchange capacity (CEC) of the biotite was measured using the NH_4Ac method [29]. The experiment was done in triplicates with samples of 1 g of biotite weighed into 50ml centrifuge tubes (Oak Ridge type 3119-0050, Thermo Scientific). Then 30ml of 1M ammonium acetate (Sigma-Aldrich, 99.99%) was then added. Samples were taken from solution at progressively increasing time intervals of 1, 2, 4, 8, 16 and 32 days. The samples were continuously rotated during this period. Phases were separated before each sampling by centrifugation at 29000g for 30 min, utilizing a centrifuge (Avanti J26S XP, Beckman Coulter). To possibly achieve further phase separation a 0.45µm polyethersulphone (PES) filter (Acrodisc IC, Pall) was used to filter the supernatant. The supernatant was then diluted 10 times with 0.5M HNO_3 (Merck, Suprapur) and analyzed with an Inductively Coupled Plasma Optical Emission Spectroscopy (ICP-OES) instrument (iCAP XP Pro, Thermo) for the content of the cations of Na, K, Mg and Ca. A series of standard solutions in the range of 1-200 ppm of these elements were made from 1000ppm stock solutions (Inorganic Ventures). An internal standard of 5 ppm Y was added to both samples and external standards.

The CEC was calculated as the sum of the major cations Na^+, K^+, Mg^{2+} and Ca^{2+} with

$$\mathrm{CEC_M}\ \left(\frac{cmol_C}{\mathrm{kg}}\right) = \frac{\mathrm{C_M \cdot V}}{\mathrm{M_s}}\ 10 \qquad \text{Eq. (1)}$$

Where C_M (M) is the measured concentration, V(L) is the volume of the leachate and M_s (g) is the total mass of the biotite mineral. The total CEC in unit $cmol_C/kg$ of exchangeable cations was calculated as

$$CEC_{tot} = CEC_{Na^+} + 2\,CEC_{Mg^{2+}} + CEC_{K^+} + 2\,CEC_{Ca^{2+}} \qquad \text{Eq. (2)}$$

2.3 Measurement of acidic site density (ASD) by tritium uptake

The tritium exchange method [30] was used to determine the acidic site density (ASD) of biotite. A solution of 120mL 52MBq/mL tritiated water (HTO) was prepared from diluting about 4mL of a stock solution of 1.57GBq/mL HTO. In four 50mL centrifuge tubes (Oak Ridge type 3119-0050, Thermo Scientific) two 5g portions of biotite of 0.25-0.5mm and two 5g portion of 0.063-0.125mm size fractions were dispersed respectively with 20ml of 52MBq/mL HTO each. In addition, two blanks were prepared. The six samples were left for about 3 months with intermittent end-over-end mixing. The excess tritiated water was then removed after centrifugation (Avanti J26S XP, Beckman Coulter) of the tubes at 29000g for 30 min. The wet mineral in the centrifuge tubes was then left in fume hood on a heating plate for initial drying. Then the tubes were placed in a vacuum chamber (Vacucell, MMM Group) at < 40mbar at room temperature. The weight of tubes was checked within intervals until a constant weight was attained, to ensure complete dryness. To the dry tubes, with and without biotite, was then added a solution of 15mL of ultrapure water (Milli-Q Advantage, Merck) and 0.1mL of 1M NaOH (Titrisol, Merck). The tubes were placed on a continuous end-over-end shaking apparatus for 57 days. During this time samples were taken intermittently by taking out 1 mL portions of supernatant after centrifugation for LSC (1414Guardian, PerkinElmer) measurement. The instrument count efficiency (cps/Bq) was determined separately to 70% for HTO. Finally, the biotite acidic site density N_H (moles/m^2) was calculated for the two size fractions with the formula:

$$N_H = \frac{A - A_w}{S_{HTO} \cdot SSA_{BET} \cdot m}\ \text{moles}\ m^{-2} \qquad \text{(Eq. 3)}$$

A(cpm) is the total measured radioactivity in the solution, compensated for previous sample outtakes, A_w is the corresponding value for blank tubes, S_{HTO} (cpm/mol) is the specific activity of the HTO solution, SSA_{BET} (m^2/g) is the BET specific surface area and m(g) is the mass of biotite.

2.4. Conditioning of biotite into Na form

Before use in titration and batch sorption experiments, the biotite was converted into the Na form. In this ion-exchange process, the crushed biotite together with 0.1 M, 0,01M, 0.001 M $NaClO_4$ (Merck, 98%) solution was put into 10 ml polypropylene tubes (Oak Ridge type 3119-0010, Thermo Scientific) and conditioned for 1.5 months. During this period of time, the electrolyte solutions were changed three times. The solution was then analyzed for exchangeable cations with ICP-OES (Thermo iCAP Pro XP Duo), by calibrating the instrument with standard solutions of Na, K, Ca and Mg.

2.5 Titration on biotite for surface pK_a values

A continuous titration on suspensions of biotite in $NaClO_4$ solutions was performed in triplicates to study the acid-base properties of biotite mineral. The titrations were made with standard solutions of 0.01M HCl as initial additive and 0.1M NaOH (both Titrisol, Merck) as a titrant, the latter was prepared and stored inside a glovebox of inert atmosphere. The titration was performed in a closed glass vessel with a computer program controlling the amount and the time of addition with an automatic titration instrument (905 Titrando, Metrohm) and with glass electrode (6.0250.010, Metrohm). The temperature of the glass vessel was fixed at 25°C, controlled by a water circulation bath (TC120, Grant). For the titration, 0.5 g of mineral was dispersed in 50ml of 0.001M $NaClO_4$ electrolyte solution. The suspension was stirred for 10 min, then HCl solution was added to give pH ~ 3. The suspension was then titrated with 0.1M NaOH with a fixed incremental volume of 4 µl/addition. A 15 min delay between additions was chosen to give a stable value after each addition. Before each titration run the electrode was calibrated with a Gran-titration procedure [31]. It has been observed in literature that solid-suspension titrations are usually carried out with the S:L ratio of 10g/L [32], [33]. According to these studies it was also found that with a too high S:L ratios, there is a possibility to have an inhomogeneous suspension which might reduce the access of surface H^+. At a too low S:L ratio, there is a risk of having too little influence from the solid phase on the measured pH. In this work the recommended S:L ratio of 10g/L was therefore selected.

2.6 Measurement of pHIEP

The isoelectric point pH_{IEP} of biotite was determined at 25 °C, using a zeta potential analyzer (Zetaphoremeter IV, CAD instrumentation) for measuring electrophoretic mobilities. To begin the experiment, a 0.1g of crushed biotite was added to a 0.001 M $NaClO_4$ solution (Merck, 98%). A total of 24 samples were prepared, spanning pH values from 2 to 9, in triplicates. The pH of the samples was adjusted using 0.1 M NaCl or $HClO_4$, and all measurements were completed within 30 minutes. The instrument uses the Smoluchowski equation [34] to calculate the zeta potential (ζ) from electrophoretic mobilities.

2.7 Batch sorption experiments

For evaluating Cs, Ba, Co and Eu sorption on the Na-converted biotite, electrolyte solutions of 0.1M, 0.01M, and 0.001M $NaClO_4$ (Merck, 98%) were prepared. These solutions were buffered to pH 5 and 9 with 1,4-Diethylpiperazine (DEPP, Alfa Aesar, 98%) , pH 6 with 2-(N-Morpholino)ethanesulfonic acid (MES, Sigma-Aldrich, 99%), pH 7 with 3-(N-Morpholino) propanesulfonic acid (MOPS, Sigma-Aldrich, 99.5%) and pH 8 with 1,4-Piperazine-bis-(propanesulfonic acid) (PIPPS, Merck, 98%). These organic buffers are recommended for their inertness towards metal complex formation [35].

The pH values were measured with a glass electrode and pH meter (pHC3006-9, PHM240, Radiometer) and were adjusted with aliquots of 0.1 M NaOH or $HClO_4$. The buffer concentrations were 5mM for 0.1 M, 0.01 M, and 0.5mM for 0.001 M $NaClO_4$ solutions, respectively. The solutions were then spiked with a mixture of acidic solutions of ^{134}Cs (CsCl in 0.1 M HCl, ^{133}Ba ($BaCl_2$ in 0.1 M HCl), ^{60}Co ($CoCl_2$ in 0.1 M HCl) and ^{152}Eu ($EuCl_3$ in 0.5

M HCl), all were 10μg /mL in carrier (Eckert & Ziegler) to obtain concentrations of ~10^{-8} M for the respective element. pH was then re-adjusted with 0.1 M NaOH or $HClO_4$ and re-measured after about 2 months, after the conclusion of the sorption experiments.

The 15 different (five pH values, three ionic strengths) spiked solutions were degassed in a glovebox antechamber for several days. Batch experiments were prepared with 0.1g of biotite in acid-washed 10ml polypropylene centrifuge tubes (Oak Ridge type 3119-0010, Thermo Scientific). The batch samples were equilibrated with 5mL 0.001, 0.01 or 0.1 M neutral $NaClO_4$ solutions for about 1 month, then centrifuged at 45000g (Avanti J26S XP, Beckman Coulter) and supernatants were removed. The tubes were then transferred into a N_2-filled glovebox with an automatic oxygen-removal system ([O_2] <1ppm, UNILab, MBraun) to minimize the formation of possible carbonate complexes.

5mL of radioactive pH-buffered electrolyte solution was added to each batch to achieve a solid-to-liquid ratio of 1:50. The batch experiments were made in triplicates, in total 45 batch experiments were prepared. In addition, 15 blank experiments for wall sorption measurements were prepared. Also, two acidified references were prepared for each radioactive solution, these were used for measurement of averaged reference radioactivity-concentration values. The sorption experiment was conducted at an ambient temperature of about 22-25°**C** for about two months, with samples taken after 2, 14, 30, and 60 days. Before each sampling, the tubes were centrifuged at 45000g for 30 min and an aliquot of 0.1ml (2% of total volume) from the supernatant was taken and mixed with 0.4ml 0.1 M HCl solution, except for the last sampling where 0.5ml was taken without any addition of acid. The gamma activity of the radionuclides in the aqueous phase was measured for 3 hours with a HPGe detector (GEM23195 detector, 2002C preamp, DSA2000 MCA, GammaAnalyst sample changer and Genie2000 v.3.4.1 software, Canberra/Mirion).

The radioactivity-based wall sorption-corrected distribution co-efficient R_d (m^3/kg) on biotite for each radionuclide was calculated with the following two equations, based on a deduction given in [36]:

$$R_d = \left(\frac{\bar{C}\cdot V_{ref}\cdot V_{out,n}}{A_{out,n}} - \left(V_0 - \sum_{i=1}^{n-1} V_{out,i}\right) - L_d - \frac{V_{out,n}\cdot\sum_{i=1}^{n-1} A_{out,1}}{A_{out,n}}\right)\cdot\frac{1}{m} \qquad \text{(Eq.4)}$$

In (Eq.4) $\bar{C}$(cpm/L) is the average measured reference concentration, taken from the acidic references, V_{ref} (L) is the initially added volume of the radioactive solution, $V_{out,n}$ (L) and $A_{out,n}$ (cpm) are the volume and measured activity of sample n of the one to n consecutive samples. V_0(L) is the initial liquid volume of the batch, which includes V_{ref} and a residual amount of liquid from the preconditioning. L_d (L) is a factor compensating for wall sorption, measured in the separate blank series of batch experiments and m(g) finally, is the mass of the solid in the sorption experiment. The two summation terms in (Eq.4) stem from an overall mass balance and they compensate for volumes and radioactivity that have been taken out in the consecutive samplings. The wall sorption factor L_d is calculated with essentially the same equation, however, since the mass participating in wall sorption is unknown, the wall sorption factor L_d (m^3) is a volume defined as

$$R_{d,wall} \cdot m_{wall} = \left(\frac{\bar{C} \cdot V_{ref} \cdot V_{out,n}}{A_{out,n}} - \left(V_0 - \sum_{i=1}^{n-1} V_{out,i} \right) - \frac{V_{out,n} \cdot \sum_{i=1}^{n-1} A_{out,1}}{A_{out,n}} \right) \equiv L_d \qquad \text{(Eq.5)}$$

2.8 Modelling Methods

2.8.1. Modelling of radiotracer uptake by particles

Depending on the configuration, batch sorption experiments may require a time period of several weeks, sometimes months, to attain equilibrium R_d values. During the initial phase, the measured R_d values are steadily increasing and only apparent, presumably due to an ongoing in-diffusion process into the porosity of the solid phase. Then, an alternative to evaluate final R_d at equilibrium one may therefore use an in-diffusion transport model to evaluate both R_d and the effective diffusivity D_e (m^2/s) from the time-dependent data, that is, to use a solution to Fick´s equation for the particular geometry.

In this case it assumed that the solid particles can be approximated to have spherical geometry and that the source is limited. A case for one sphere is described by [37] and a solution is given for the time-dependent concentration in solution. Since not one but a number of particles n_s are involved in a batch experiment, the solution must be modified with this factor into:

$$C_t = C_0 \cdot \left[1 - \left(\frac{C_0 - C_\infty}{C_0} \right) \cdot \left[1 - \sum_{i=1}^{\infty} \frac{6z(1+z)}{9+9z+z^2 q_i^2} \cdot e^{\left(-\frac{D \cdot q_i^2 \cdot t}{n_s \cdot r^2} \right)} \right] \right] \qquad \text{(Eq.6)}$$

C_t, C_0 and C_∞ are the momentarily, initial and final concentration in solution, respectively, z is defined as

$$z = \frac{C_\infty}{C_0 - C_\infty} = \frac{V}{n_s \cdot \alpha \cdot V_p} \qquad \text{(Eq.7)}$$

The second equality in (Eq.7) includes solution and particle volumes V and V_p, respectively, and the capacity factor. This equality can be deduced from the overall mass balance.

In (Eq.6), q_i is the i:th root to

$$\tan q_i = \frac{3 q_i}{3 + z \cdot q_i^2} \qquad \text{(Eq.8)}$$

In (Eq.6) r(m) is the particle radius and D (m^2/s) is the apparent diffusivity, which is related to D_e and the capacity factor by

$$D = \frac{D_e}{\alpha} = \frac{D_e}{(\varepsilon + K_d \cdot \rho)} \qquad \text{(Eq.9)}$$

Here ε is the particle porosity, K_d(m^3/kg) the distribution constant and ρ(kg/m^3) the particle density. For the modelling of the uptake, the fitting parameters to (Eq.6) are D_e and α. The factor n_s is estimated from the assumed spherical shape and the weighed-in mass of the particles in each batch. For the evaluation of K_d (~ R_d) from the capacity factor, the porosity of the

particles is assumed to be negligible.

2.8.2. Modelling of sorption and titration data

For the modelling of the sorption and titration data, a conceptual model of biotite was used, pictured in Fig.1.

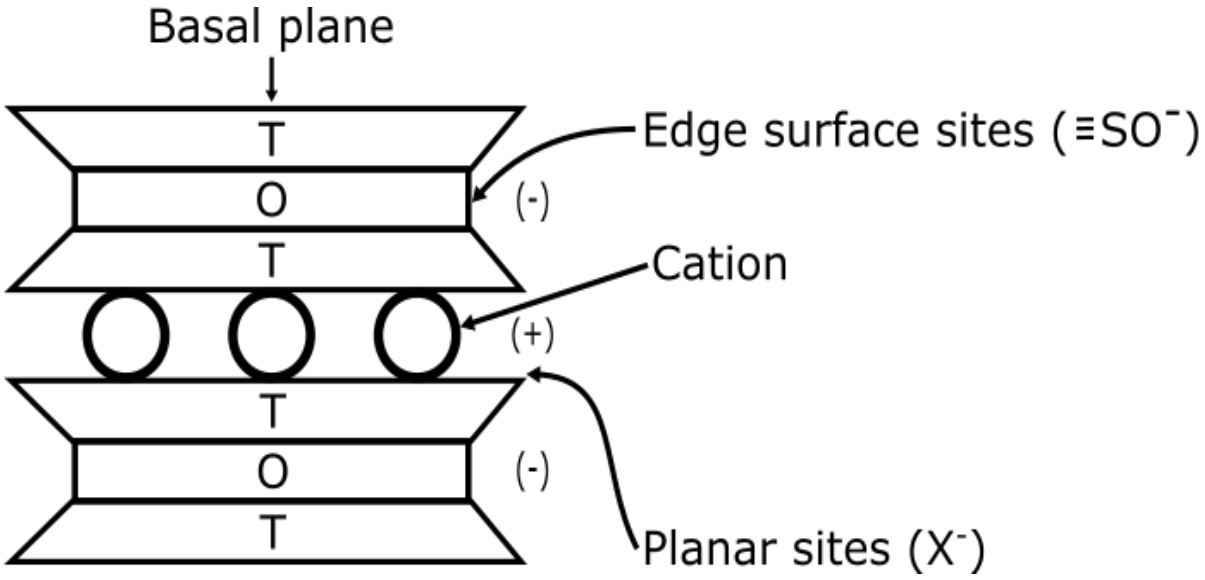

Fig.1. Conceptual model of biotite

This conceptual model is based on the structure of biotite and the evidence from literature sorption data that there should exist, at least, one cation exchange site (X) and one surface complexation site ($\equiv SO^-$) to explain the measured sorption data. In a reasoning based on the known biotite structure, in this concept the exchange sites are assumed to be located at basal planes, while complexation sites are located at the edges. Also based on literature review on the dissolution characteristics of sheet silicates [18], the surface complexation sites ($\equiv SO^-$) are, more specifically, considered to:1) be acidic 2) consist of silanol or aluminol terminal groups, and 3) participate in the following de-protonation reactions:

$$\equiv SiOH \rightleftharpoons \equiv SiO^- + H^+$$

$$\equiv AlOH_2^+ \rightleftharpoons \equiv AlOH + H^+$$

$$\equiv AlOH \rightleftharpoons \equiv AlO^- + H^+$$

According to this concept, surface charge is present at the biotite edges, while the basal planes are kept neutral by the exchange process. The edges constitute less than about 10% of the surface area according to FEG-SEM studies on different particle size fractions [38],. Moreover, one may also consider the trace concentrations of cationic elements used here, which means that surface complex concentrations are, at all pH values, well below the site concentrations, the difference is about 3 orders of magnitude. The approach here is therefore to use a non-electrostatic SCM, which does not consider any build-up of positive charge on the surface edges due to the sorption of cations that repel further sorption.

To model sorption, it is necessary to establish some basic parameters of the biotite mineral, namely the total acidic site density (ASD) and the cation exchange capacity (CEC). These parameters limit the number of surface complexation and cation exchange sites, respectively and the parameters were determined in separate experiments, described above. The other vital characteristic of biotite for modelling of its sorption properties is to determine the pK_a values for the surface complexation sites, the aforementioned silanol and aluminol groups. This is mainly done by the method of titration on suspensions of the solid phase, described above. However, one can expect that silanol groups much behaves like silica mineral with a point of zero charge about pH 3 [39] and consequently a pK_a about this value. This pK_a is too low to be detected in a titration experiment with hydroxide on an acidified suspension, that starts about pH 3.5. Instead, the iso-electric point (IEP) measurement was used to deduce the pK_a value for silanol. On the other hand, typical values of point of zero charge for alumina are in the pH 4-8 range (*ibid.*) and aluminol pK_a values should consequently be possible to deduce from the titration.

The specific surface area (SSA) was mainly used for normalizing the Acidic Site Density measurements. However, SSA can also be useful if one would like to normalize weight-specific values, for example, to convert the R_d (m^3/kg) values to surface normalized R_a(m) values, particularly if one would like to compare the results obtained here with other biotite sorption datasets. It is not likely that SSA measured with gas-adsorption BET captures the interlayer surfaces. This has been demonstrated when compared with liquid adsorption methods like the EGME (ethylene glycol monomethyl ether) method for clay minerals [40].

The titration data was modelled by including the following reactions:

$$NaX + H^+ \rightleftharpoons HX + Na^+ \quad \text{(R.1)}$$
$$\equiv SOH \rightleftharpoons \equiv SO^- + H^+ \quad \text{(R.2)}$$
$$\equiv SOH_2 \rightleftharpoons \equiv SOH + H^+ \quad \text{(R.3)}$$
$$\equiv SO^- + Na^+ \rightleftharpoons \equiv SONa \quad \text{(R.4)}$$
$$\equiv SOH + Na^+ \rightleftharpoons SOHNa^+ \quad \text{(R. 5)}$$

The reactions consider, in turn, ion-exchange on basal planes between protons and cation of electrolyte (R.1), protonation of edge surface (R.2 and 3) and a strong (R.4) and a weak (R.5) surface complex with cation, in this case from electrolyte. The corresponding selectivity co-efficient for ion-exchange K_{NaX} is defined by:

$$\mathrm{K}_{NaX} = \frac{[HX]\{Na^+\}}{[NaX]\{H^+\}} \quad \text{(Eq. 10)}$$

The surface acidity constants K_{a1} and K_{a2} are defined as

$$\mathrm{K_{a1}} = \frac{[\equiv \mathrm{SOH}]\{\mathrm{H^+}\}}{[\equiv \mathrm{SOH_2}]} \quad \text{(Eq.11)}$$

$$\mathrm{K_{a2}} = \frac{[\equiv \mathrm{SO^-}]\{\mathrm{H^+}\}}{[\equiv \mathrm{SOH}]} \quad \text{(Eq. 12)}$$

The surface complexation constants for the reactions (4) and (5) are

$$\mathrm{K}_{SONa} = \frac{[\equiv \mathrm{SONa}]}{[\equiv \mathrm{SOH}]\{Na^{+}\}} \quad \text{(Eq.13)}$$

$$\mathrm{K}_{SOHNa} = \frac{[\equiv \mathrm{SOHNa}^{+}]}{[\equiv \mathrm{SOH}]\{Na^{+}\}} \quad \text{(Eq.14)}$$

Where, the symbol [] indicates the concentration is given in unit mol/L. For the titration data the model was fitted by minimizing the error sum

$$\sum_{i=1}^{n} abs(\{H^{+}\}_{exp,i} - \{H^{+}\}_{calc,i}) \quad \text{(Eq.15)}$$

In (Eq.15) *n* is the number of steps in the titration curve, $\{H^{+}\}_{exp,i}$ is the measure proton activity at point *i* and $\{H^{+}\}_{calc,i}$ is the calculated proton activity according to the mass balances:

$$\frac{V_{HCl} \cdot C_{HCl} - V_{NaOH} \cdot C_{NaOH}}{V_{tot,i}} = [H^{+}] - [OH^{-}] + [HX] + [\equiv SOH] + 2 \cdot [\equiv SOH_2] - [NaX] \quad \text{(Eq.16)}$$

$$\frac{CEC \cdot m_{biotite}}{V_{tot,i}} = [HX] + [NaX] \quad \text{(Eq.17)}$$

$$\frac{ASD \cdot m_{biotite}}{V_{tot,i}} = [\equiv SO^{-}] + [\equiv SOH] + [\equiv SOH_2] + [\equiv SONa] + [\equiv SOHNa^{+}] \quad \text{(Eq. 18)}$$

$$\frac{[Na^{+}]_{NaClO4} \cdot V_{NaClO4} + [Na^{+}]_{NaOH} \cdot V_{NaOH,i}}{V_{tot,i}} = [Na^{+}] + [NaX] + [\equiv SONa] + [\equiv SOHNa^{+}] \quad \text{(Eq.19)}$$

Here *CEC* and *ASD* are the measured cation exchange capacity and acidic site density in moles/g, respectively. $m_{biotite}$ is the mass of biotite in the titration and $V_{tot,i}$ is the total volume at titration point *i*. This equation system, with the four "master species" H^{+}, Na^{+}, HX and $\equiv SO^{-}$ as variables together with (Eqs. 10-14) is solved for each titration point with the PHREEQC software [41]. The initial contribution of H^{+} and Na^{+} from the biotite itself to (Eq. 10) and (Eq.13), respectively, were judged to be negligible compared with the amounts added as solutions at the start of titration.

The optimization of the model was accomplished by coupling the PHREEQC [41] chemical speciation software with a PYTHON optimization routine through an integration code [42] [43]. This code is a Microsoft COM (component object model) version of PHREEQC called IPHREEQC and facilitates a link to communicate and interchange the data between PHREEQC and other software like Excel, MATLAB and programming languages such as PYTHON, and

Visual Basic. The optimization parameters are the assumed reaction constants and partitioning coefficients, as defined in (Eqs 10-14). One may also note that these are treated in PHREEQC as valid at zero ionic strength and that activity coefficients are applied to all dissolved species by the program, according to the given ionic strength.

With several parameters fixed from modelling of titration, that is, the equilibrium constants and coefficients in (Eqs. 10-14), a similar model was fitted to the radionuclide distribution coefficients R_d obtained from modelling radionuclide in-diffusion into biotite particles, as described in previous section, in the batch sorption experiments.

$$\sum_{i=1}^{n} abs(R_{d,exp,i} - R_{d,calc,i}) \quad \text{(Eq.20)}$$

Here *n* denotes the number of batch experiments for one radiotracer, which were 45 in total (5 pH, 3 ionic strengths, triplicates). Similar reactions for ion exchange (R.1) and surface complexation (R.4 and 5) were used for the radiotracer cations. However, here also hydroxide complex formation had to be considered. The hydroxide complexes included in the model are shown in Table 1, below.

Table 1: Thermodynamic data of aqueous hydroxide complexes of Ba, Co, and Eu used in sorption modeling.

Reaction	**log_β**
$\mathbf{Ba^{2+} + H_2O = Ba(OH)^{+} + H^{+}}$	0.65[a]
$\mathbf{Co^{2+} + H_2O = Co(OH)^{+} + H^{+}}$	4.39[b]
$\mathbf{Co^{2+} + 2H_2O = Co(OH)_2 + 2H^{+}}$	8.23[b]
$\mathbf{Co^{2+} + 3H_2O = \boldsymbol{Co(OH)_3^{-}} + 3H^{+}}$	10.0[b]
$\mathbf{Eu^{3+} + H_2O = Eu(OH)^{2+} + H^{+}}$	6.4[b]
$\mathbf{Eu^{3+} + 2H_2O = Eu(OH)_2^{+} + 2H^{+}}$	12.3[b]
$\mathbf{Eu^{3+} + 3H_2O = Eu(OH)_3^{0} + 3H^{+}}$	17.1[b]

[a]PHREEQC database MINTEQ [b][44]

Some hydroxide complexes of radiotracers were allowed to form surface complexes, and, in some cases, exchange species and corresponding reactions and reaction constants were defined according to same formalism as for the cations. The hydroxide surface species are described further in the results.

Mass balances for the batch sorption modelling were also similar to those shown for titration modeling, except that both volume and pH were assumed to be constants. The latter condition means that a mass balance for protons (Eq.16) and the corresponding H^+ master species were not necessary to include in model.

3. Results and Discussion

3.1. Characterisation of biotite mineral

The specific surface area (SSA) of biotite 0.25–0.5mm size fraction was measured with the Kr-BET analysis to 0.47±0.01m^2/g. For comparison, a value of 0.83m^2/g was obtained with N_2-BET of the same particle size fraction of a Finnish biotite specimen by [20]. There can be many explanations for this discrepancy, including the use of different gases to measure surface area, where Kr-BET is considered to be more accurate for low SSA (<1m^2/g). Natural variations in biotite and the crushing and cleaning processes can also play a role in the discrepancy. Our measured value for the 0.075-0.125mm size fraction was 1.12 m^2/g, and this can be compared with a value of 1.03m^2/g for a 0.075-0300mm size fraction of Finnish biotite specimen, measured by [24].

The measurement of cation exchange capacity (CEC) of the biotite mineral gave a value of 1.03±0.03cmol$_C$/kg. This value can be compared to literature data of a Finnish biotite specimen, 16.3 cmol$_C$/kg for a similar size fraction [20] and 1.26 cmol$_C$/kg for a 0.075-0300mm size fraction, measured by [24]. CEC values for three Finnish biotite specimen of unknown size fractions are given by [25] and are in the range of 1.3-1.7cmol$_C$/kg. Except for the value measured by [20] the CEC values for the different biotite specimen seem to be fairly consistent.

The aim of the tritium exchange method is to evaluate the extent of tritium protons exchanged with protons accessible on the mineral surface for a measurement of Acidic Site Density (ASD) at neutral pH. A neutral pH was preferred since this will minimize biotite dissolution. The results of the four experiments of two size fractions in duplicates are shown in Fig. 1.

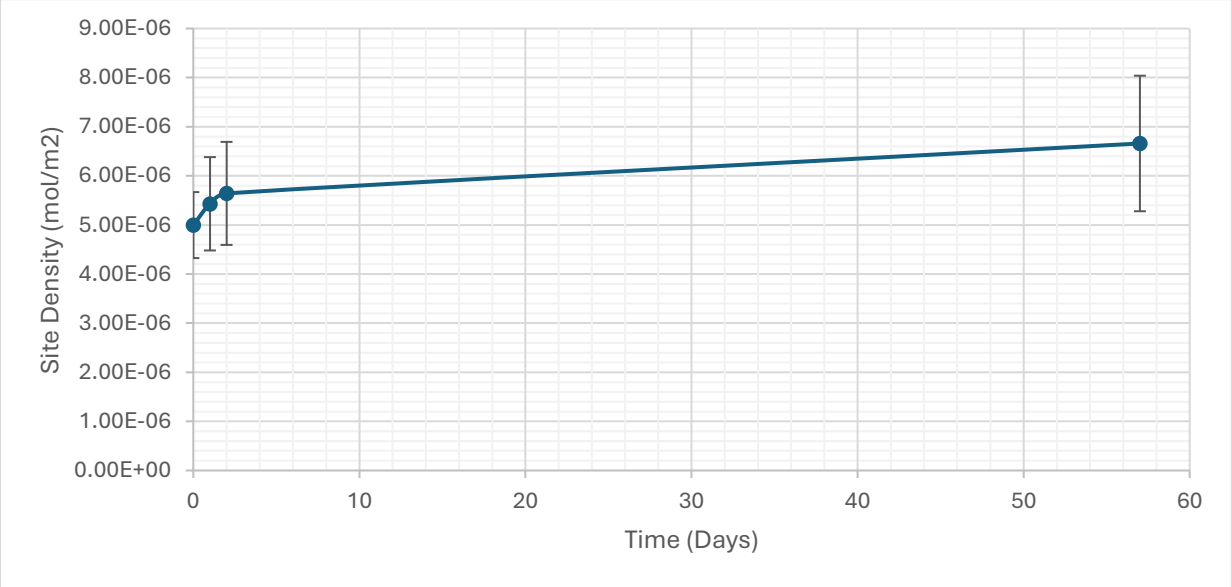

Figure 1. Results of tritium exchange experiement for acidic site density (ASD of biotite, average of four measurements

The results indicate that the majority of tritium exchange with biotite surface water occurs within the first few days. After that, the exchange rate slows down significantly and eventually

reaches an almost constant level. The calculated average site capacity is 3.14±0.27μmol/g. However, at neutral pH this site density accounts only for the singly protonated aluminol sites. Here one must also consider silanol sites that are completely de-protonated (expected pKa~3, or at least below the pKa1 of the aluminol sites) at neutral pH and are hence not detected with the method. If one considers a silanol to aluminol site ratio of 2.6:1.3, according to the Si:Al ratio of the biotite composition, the experimental value should be multiplied with a factor of 3 for a total ASD of 9.42±0.71μmol/g.

To the best of our knowledge, any experimental ASD values for biotite have not been reported in literature but it has been used as fitting parameter in titrations on biotite suspensions by [25], which gave 64μmol/g for a 1-pKa model, or 32μmol/g for a 2-pKa model. Both values are considerably larger than our experimental data. The parameter has also been estimated by DFT calculations to 7.6μmol/g for a Finnish biotite [24], a value which is close to our experimental data. This calculated total ASD value was based on two types of edge sites (element was not specified) in the proportion 3.2:1.4, while the analyzed Si:Al ratio of the Finnish biotite was reported to be 2.9:1:1. The close similarity in the DFT modelled ratios for two type of sites and the analyzed Si:Al ratio of biotite supports the assumption that the latter ratio can be used as an estimation of the silanol:aluminol site ratio and may therefore also be used for an adjustment of the ASD value obtained from the tritium uptake experiments at neutral pH.

The zeta potential measurements of the 0.25–0.5mm size fraction biotite fraction gave a pH_{IEP}= 3.0. This value agrees well with a pH_{IEP}=3.02 for a <53μm size fraction of biotite reported by [34].

After conditioning of biotite with 0.01 M and 0.001 M $NaClO_4$ for the use in titration and sorption experiments, the K was steadily decreasing in the solution, giving a biotite that was 80% converted from K to Na form, however, in the case of 0.1 M $NaClO_4$, the conversion was only 31%.

3.2. Titration results

The titration curve is shown in Fig 2 (pH vs. added base) and the optimized reaction constants in Table 2.

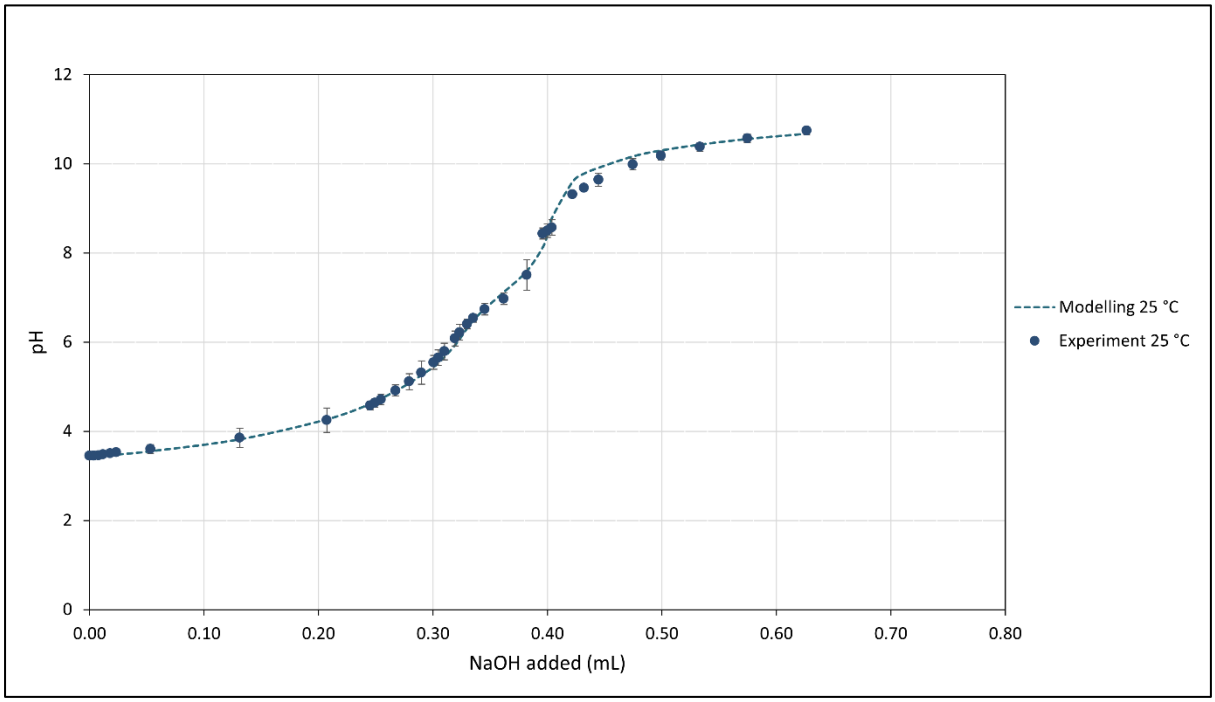

Figure 2. Experimental (points, average of triplicates) and modelled (line) titration curve for a suspension of biotite in 0.01 M $NaClO_4$ at 25°C

Table 2. Optimized reaction constants/coefficients with the optimized Acidic Site Density and Cation Exchange Capacity for biotite in 0.01 M $NaClO_4$.

Surface complexation reactions	**Constants (log_K)**
$\equiv \mathbf{SOH_2} \rightleftharpoons \equiv \mathbf{SOH} + \mathbf{H^+}$	-4.9 ± 0.1
$\equiv \mathbf{SOH} \rightleftharpoons \equiv \mathbf{SO^-} + \mathbf{H^+}$	-7.1 ± 0.2
$\equiv \mathbf{SOH} + \mathbf{Na^+} \rightleftharpoons \equiv \mathbf{SONa} + \mathbf{H^+}$	1.6 ± 0.1
$\equiv \mathbf{SOH} + \mathbf{Na^+} \rightleftharpoons \equiv \mathbf{SOHNa^+}$	0.5 ± 0.1
Cation exchange reaction	**Coefficient (log_K)**
$\mathbf{Na - X} + \mathbf{H^+} \rightleftharpoons \mathbf{H - X} + \mathbf{Na^+}$	3.0 ± 0.2
Total site capacities	**Site densities (mol/g)**
Acidic Site density (optimized)	$1.7 \pm 0.1 \times 10^{-5}$
Cation Exchange Capacity (optimized)	$2.6 \pm 0.4 \times 10^{-5}$

In order to obtain the best fit, the ASD and CEC values were also allowed to be optimized along with the reaction constants and coefficients. The values are somewhat larger than the experimental values, the ASD a factor of 1.7 and the CEC a factor of 2.6 larger. The reason for this discrepancy is not clear, but since both types of site densities were affected, one may suspect that the stirring of the suspension may have partially broken the biotite size fraction into smaller pieces, thereby yielding more surfaces than the original material. This could have been checked with a post-titration measurement of the SSA but was unfortunately not done.

However, it should not have any influence on the reaction constants and coefficient which determinations were the primary goal of the titration.

Fig. 3 shows the net proton consumption at titration as a function of pH. The point of zero charge (pH_{PZC}) for the whole system (surface and solution) is identified where the titration curve intersects with the x-axis, in this case about pH 5.8. Comparable results for a Finnish biotite were reported by [25] with a pH_{PZC}= 6. One may note that this point is different from the pH of the iso-electric point (pH_{IEP}) that indicates surface neutrality.

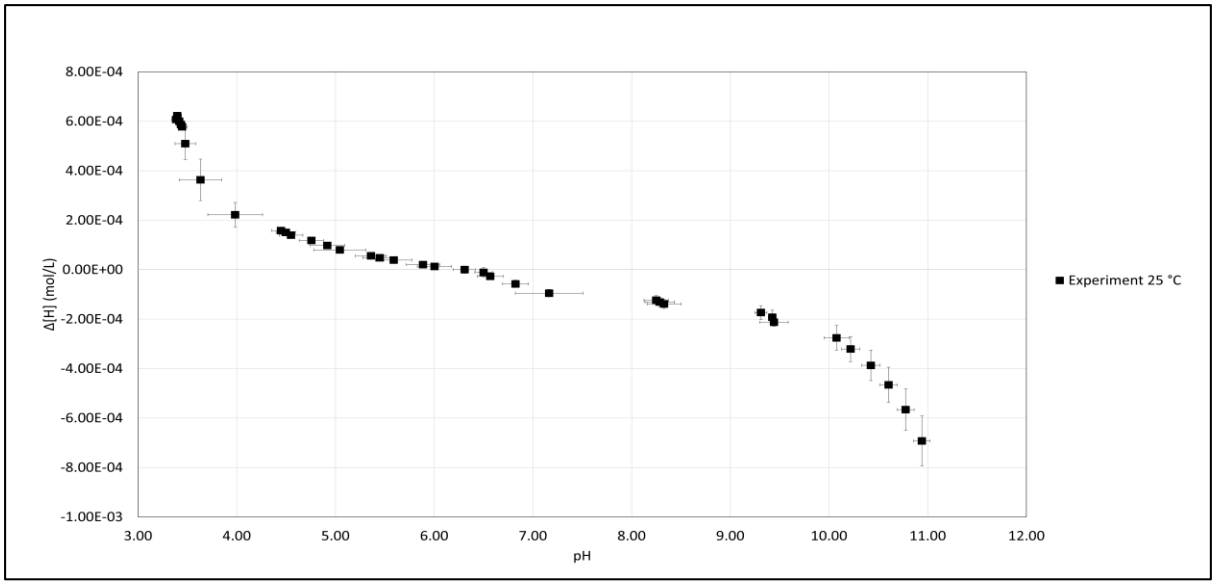

Figure 3. Potentiometric titration of a biotite suspension in 0.01 M $NaClO_4$ solution at 25°C

3.3. Batch sorption results

The fitting parameters to Eq.(6) for each series and the measured final pH in batch sorption are presented in Table 3, below. More specific results for The SCM of each radiotracer element are presented in the following sections.

Table 3. Measured final pH and fitting parameters De and Rd to Eq. (6) in batch sorption experiments.

I		**pH 5**	**pH 6**	**pH 7**	**pH 8**	**pH 9**
0.001 M	**final pH**	5.67	6.08	7.10	8.05	8.58
	$D_{e,Cs}$ **(m^2/s)**	$1.1\ 10^{-12}$	$1.5\ 10^{-13}$	$4.9\ 10^{-13}$	$2.1\ 10^{-12}$	$1.6\ 10^{-12}$
	~~$R_{d,Cs}$ **(m^3/kg)**~~	1.5	2.0	1.6	1.1	1.2
	$D_{e,Ba}$ **(m^2/s)**	$1.3\ 10^{-13}$	$2.1\ 10^{-12}$	$5.5\ 10^{-13}$	$7.9\ 10^{-13}$	$3.8\ 10^{-13}$
	$R_{d,Ba}$ **(m^3/kg)**	0.47	1.2	3.8	6.2	9.0
	$D_{e,Co}$ **(m^2/s)**	$2.7\ 10^{-12}$	$1.3\ 10^{-11}$	$5.0\ 10^{-13}$	$4.0\ 10^{-13}$	$1.5\ 10^{-13}$
	$R_{d,Co}$ **(m^3/kg)**	0.02	0.16	1.5	10	4.8
	$D_{e,Eu}$ **(m^2/s)**	$2.1\ 10^{-12}$	$6.3\ 10^{-13}$	$4.8\ 10^{-13}$	$3.2\ 10^{-13}$	$1.2\ 10^{-12}$
	$R_{d,Eu}$ **(m^3/kg)**	4.0	11	6.4	5.3	2.5
0.01 M	**final pH**	5.17	6.08	7.08	8.11	9.04
	$D_{e,Cs}$ **(m^2/s)**	$6.2\ 10^{-12}$	$1.4\ 10^{-12}$	$1.3\ 10^{-12}$	$1.0\ 10^{-12}$	$6.0\ 10^{-13}$
	$R_{d,Cs}$ **(m^3/kg)**	0.12	0.38	0.52	0.47	0.65
	$D_{e,Ba}$ **(m^2/s)**	$1.0\ 10^{-11}$	$2.8\ 10^{-12}$	$2.9\ 10^{-12}$	$1.2\ 10^{-12}$	$5.2\ 10^{-13}$
	$R_{d,Ba}$ **(m^3/kg)**	0.024	0.65	1.3	1.8	5.6
	$D_{e,Co}$ **(m^2/s)**	$6.3\ 10^{-11}$	$7.9\ 10^{-12}$	$7.2\ 10^{-13}$	$5.5\ 10^{-13}$	$5.3\ 10^{-13}$
	$R_{d,Co}$ **(m^3/kg)**	0.0065	0.095	1.7	5.9	2.4
	$D_{e,Eu}$ **(m^2/s)**	$1.1\ 10^{-11}$	$1.0\ 10^{-12}$	$4.8\ 10^{-13}$	$1.6\ 10^{-12}$	$1.1\ 10^{-12}$
	$R_{d,Eu}$ **(m^3/kg)**	0.13	3.6	5.0	9.3	1.8
0.1 M	**final pH**	5.12	6.06	7.08	8.11	9.02

	$D_{e,Cs}$ (m^2/s)	$1.1\ 10^{-11}$	$8.3\ 10^{-12}$	$4.6\ 10^{-12}$	$7.1\ 10^{-12}$	$3.4\ 10^{-12}$
	$R_{d,Cs}$ (m^3/kg)	0.044	0.12	0.14	0.13	0.14
	$D_{e,Ba}$ (m^2/s)	$1.0\ 10^{-11}$	$1.0\ 10^{-11}$	$1.0\ 10^{-11}$	$2.5\ 10^{-11}$	$3.5\ 10^{-12}$
	$R_{d,Ba}$ (m^3/kg)	0.032	0.064	0.095	0.14	0.35
	$D_{e,Co}$ (m^2/s)	$1.0\ 10^{-11}$	$1.4\ 10^{-11}$	$6.3\ 10^{-13}$	$5.5\ 10^{-13}$	$4.4\ 10^{-13}$
	$R_{d,Co}$ (m^3/kg)	0.019	0.035	0.48	2.7	1.1
	$D_{e,Eu}$ (m^2/s)	$1.0\ 10^{-11}$	$6.2\ 10^{-13}$	$2.1\ 10^{-12}$	$2.8\ 10^{-12}$	$3.0\ 10^{-12}$
	$R_{d,Eu}$ (m^3/kg)	1.1	6.4	6.4	1.9	4.7

3.3.1. Results for Cs sorption on biotite

In Fig. 4 the time-dependent data for Cs sorption on biotite in 0.001 M $NaClO_4$ is shown. An equilibrium seems to be almost established after 30 days, but values increase for the acidic pH. For pH 9, a slight decrease can be detected, this is possibly caused by biotite dissolution. The complete set of time dependent apparent R_d values for Cs sorption onto biotite is given in Table A-1 in Appendix A.

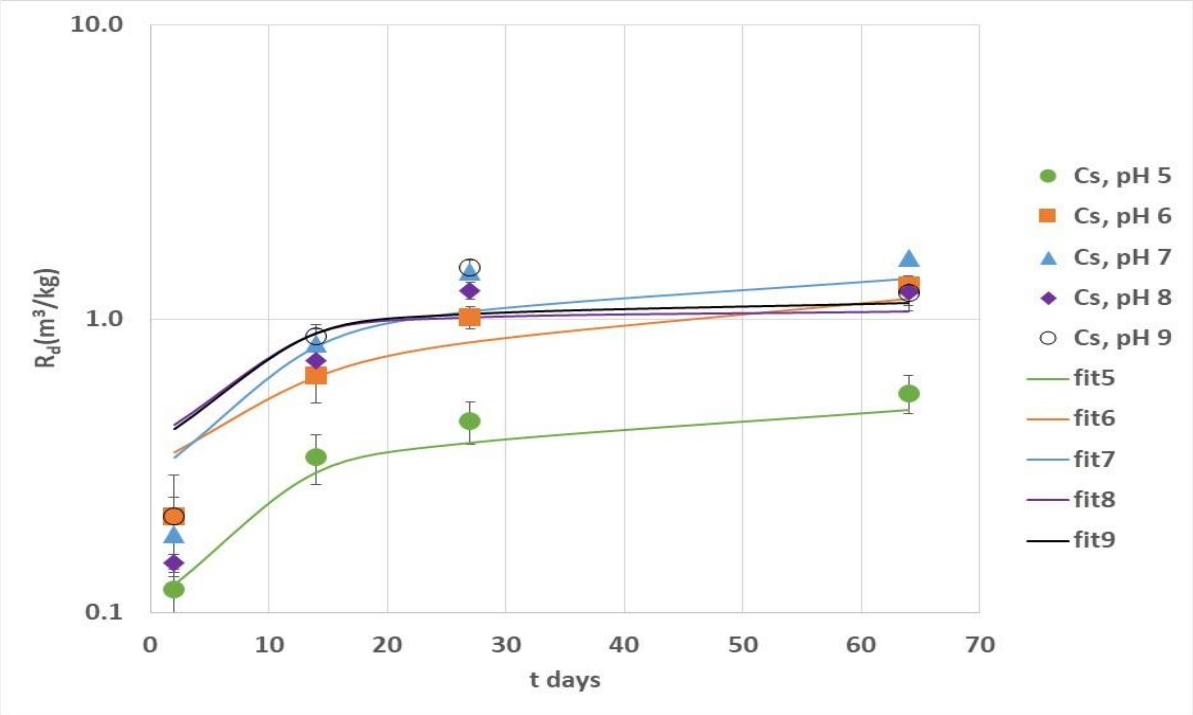

Figure 4. Measured R_d values for Cs sorption onto biotite in 0.001 M $NaClO_4$ versus time.

In Fig.5 the experimental and fitting data for the sorption of Cs on biotite in $NaClO_4$ solutions are shown. The results indicate that both pH and ionic strength have significant impact on Cs sorption: R_d values increase with pH but decrease with ionic strength. The latter decrease is primarily an effect due to the increase of competing Na^+ ions, which decrease the availability of surface sites.

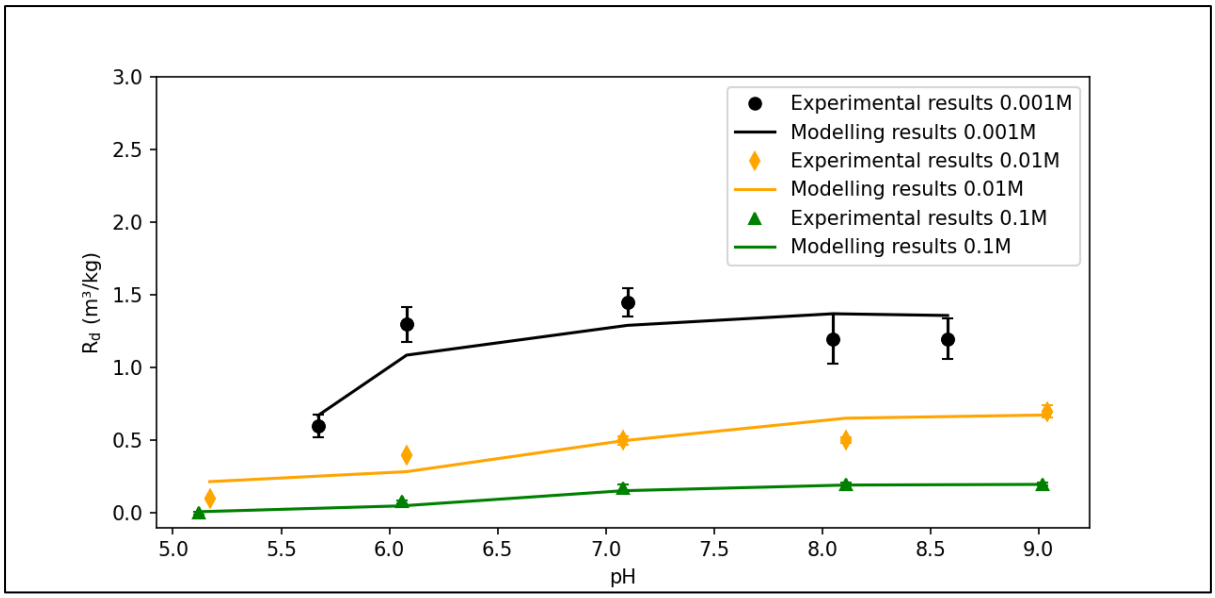

Figure 5. Cs sorption on biotite mineral in 0.001 M, 0.01 M, and 0.1 M $NaClO_4$ solutions.

In Fig.6 the different species are shown for modelling Cs sorption on biotite in 0.001 M $NaClO_4$. Figures for the other solutions are available in Appendix B.

The model was applied on the dataset where the surface species CsX, ≡SOCs, and ≡SOHCs were considered, however, the contribution of the latter was not found to improve the fitting and was therefore subsequently omitted from model.

The modelling results indicate that, at lowest ionic strength, for all pH values (5 to 9) the Cs uptake is chiefly governed by ion exchange with some contribution of surface complexation. With the other two electrolytic concentrations (0.01 and 0.1 M), it was noted that as the ionic strength increased surface complexation started to take over as the main sorption process, and at the highest electrolytic concentration (0.1 M), ion exchange was found to have a very small role in the Cs uptake. The reactions and the related constants are listed in Table 4. The cation exchange coefficient was allowed to vary with ionic strength since the exchange reaction (R.1) does probably not represent a fundamental reaction mechanism, but may consist of at least two reaction steps, this is also implicated by the use of a selectivity coefficient and not a constant.

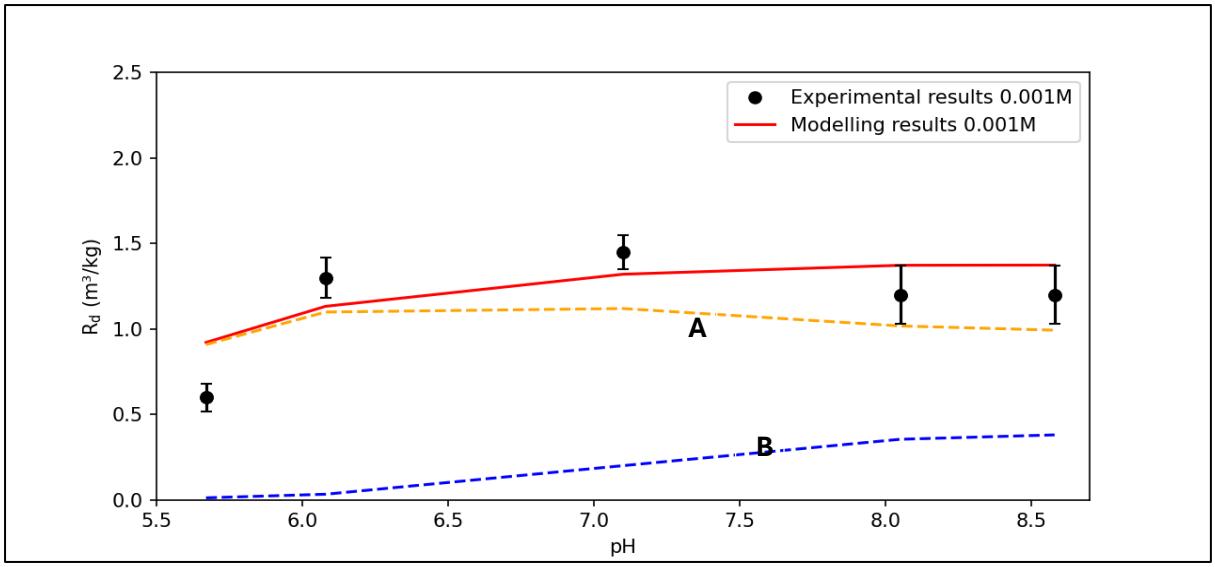

Figure 6. Cs sorption modelling results (lines) on biotite mineral in 0.001 M $NaClO_4$ solution showing the contribution of different surface speciess: (A) CsX; (B) ≡SOCs

Table 4: Surface complexation reaction and constant at zero ionic strength (log k°) for Cs.Selectivity coefficients are for the specified ionic strength

Reactions		**log k° (25°C)**	
$\equiv SO^- + Cs^+ \leftrightarrow \equiv SOCs$		4.6 ± 0.2	
$\equiv SOH + Cs^+ \leftrightarrow \equiv SOHCs^+$		Not significant*	
Reaction/Ionic Strength at 25 °C	**log k (0.001 M)**	**log k (0.01 M)**	**log k (0.1 M)**
$Cs^+ + NaX \leftrightarrow CsX + Na^+$	1.7	2.0	1.3

*Inclusion of this species gave no improvement of error sum

3.3.2 Results for barium sorption onto biotite

Sorption of Ba, time dependent results, are shown in Fig. 7. These indicates that sorption reached an equilibrium after 30 days, with a possible exception for pH 5 series which seems to keep on increasing. The complete set of time dependent apparent R_d values for Ba sorption onto biotite is given in Table A-2 in Appendix A.

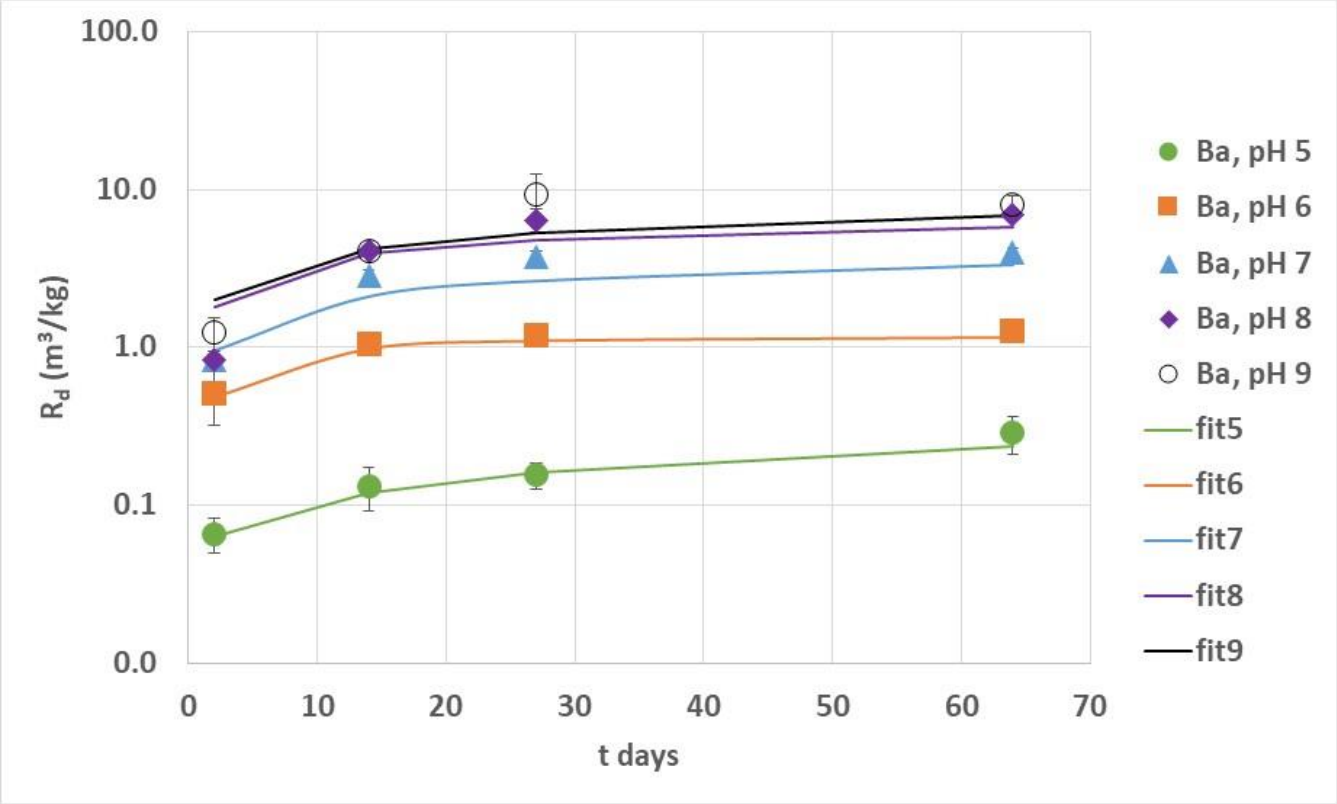

Figure 7: Measured R_d values for Ba sorption onto biotite in 0.001 M $NaClO_4$ versus time.

The data fitting results for Ba sorption on biotite as a function of pH and $NaClO_4$ concentration (0.001,0.01 and 0.1 M) are displayed in Fig.8. It was observed that the Ba sorption is highly dependent on both pH and ionic strength. For 0.01 and 0.1 M ionic strengths, the R_d-values seems to be steadily increasing from pH 5 to pH 8. However, an additional rise in Ba sorption was found between pH 8 and 9 (Fig. 8). At pH 8 to 9, the increase in Ba sorption can be due to the formation of barium hydroxyl species.

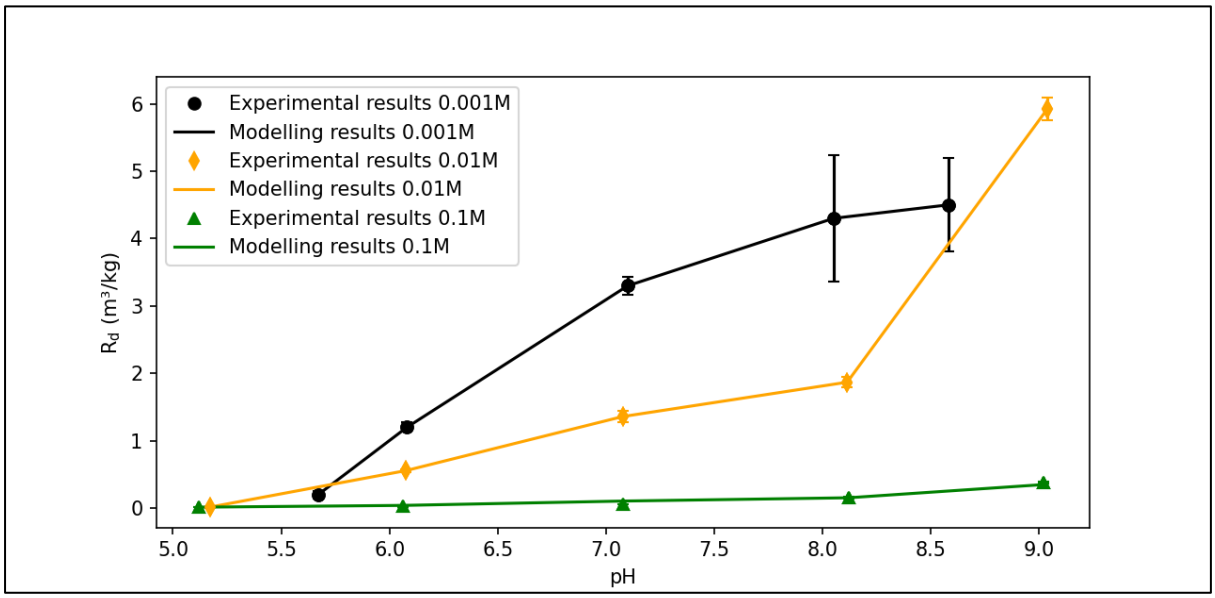

Figure 8. Ba sorption on biotite in 0.001 M, 0.01 M, and 0.1 M $NaClO_4$ solutions.

In Fig.9 the different components are shown for modelling Ba sorption on biotite in 0.001 M $NaClO_4$. Figures for the other ionic strengths are available in Appendix B.

The model was applied on the dataset with the two exchange surface species, BaX_2 and BaOHX, together with three surface complexes, $\equiv SOBa^+$, $\equiv SOBaOH$ and $\equiv SOHBa^{2+}$, although the latter was subsequently omitted from model because it was s not found to improve the fitting. Based on the model results, Ba appears to have a similar behavior to Cs, but sorption is stronger because of increased charge of cation. The results show that for 0.001 M background electrolytic concentration, Ba sorption is mainly controlled by ion exchange, as BaX_2 with some contribution of surface complexation from $\equiv SOBa^+$ and, at high pH, also $\equiv SOBaOH$ and the BaOHX exchange specie appears to have a role in Ba uptake. Furthermore, it was observed that as the ionic strength increased from 0.001 to 0.1 M, surface complexation became the primary sorption process. Table 5 shows the reactions and their constants.

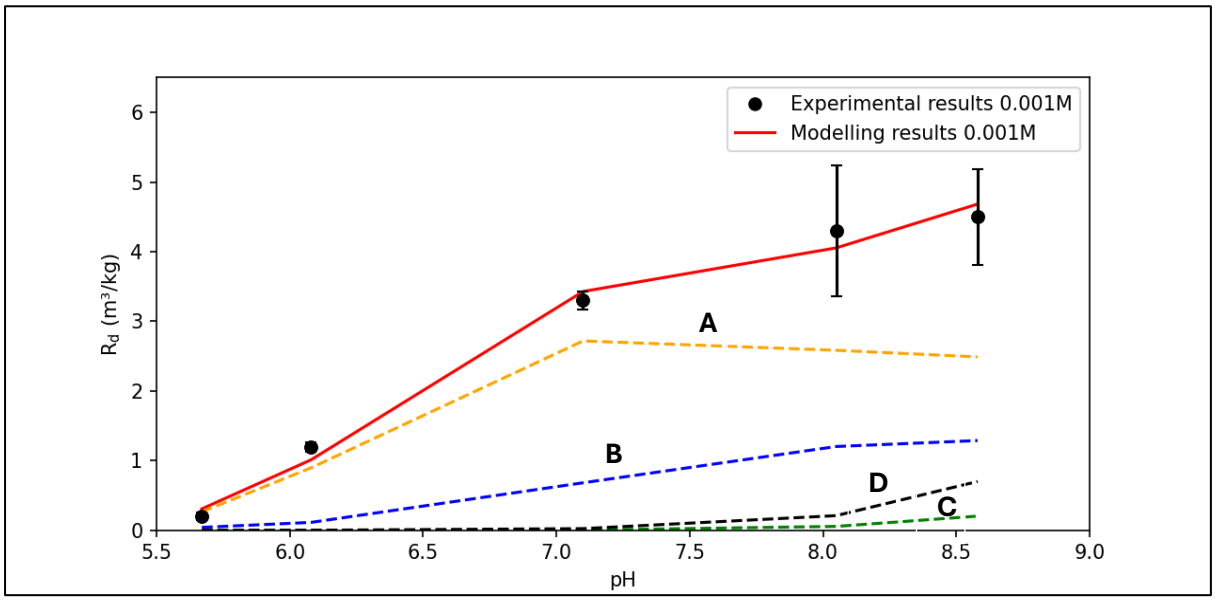

Figure 9. An example figure for Ba sorption measurement (symbol) and modelling (continuous line) on biotite mineral in 0.001 M, 0.01 M and 0.1 M $NaClO_4$ solution at 25 °C. The contribution of different Ba(II) species in its sorption is represented by different curves:(A: Yellow line) BaX_2; (B: Blue line) $\equiv SOBa^+$; (C: Green line)) $\equiv SOBaOH$; (D: Black line) XBaOH.

Table 5: Surface complexation and cation exchange reactions and their associated constants at zero ionic strength (log_k°) for Ba. Selectivity coefficients are for the specified ionic strength

Reactions		**log k° (25 °C)**	
$\equiv SO^- + Ba^{2+} \leftrightarrow \equiv SOBa^+$		5.0 ± 0.2	
$\equiv SO^- + Ba(OH)^+ \leftrightarrow \equiv SOBaOH$		9.2 ± 0.2	
$\equiv SOH + Ba^{2+} \leftrightarrow \equiv SOHBa^{2+}$		Not significant*	
$NaX + BaOH^+ \leftrightarrow BaOHX + Na^+$		7.2 ± 0.6	
Reaction/Ionic Strength at 25 °C	**log k (0.001 M)**	**log k (0.01 M)**	**log k (0.1 M)**
$Ba^{2+} + 2NaX \leftrightarrow BaX_2 + 2Na^+$	– 0.4	0.5	1.3

*Inclusion of this species gave no improvement of error sum

3.3.3. Results for cobalt sorption onto biotite

The time-dependent results for Co sorption onto biotite are shown in Fig.10, which shows that Co sorption stabilizes already after 10-15 days, although data for pH 7 shows a slight increase up to 60 days. For pH 5 a slight decrease is indicated, possibly showing influence of biotite dissolution. It was therefore decided to ignore the last point in time-dependent modelling of Co sorption for pH 5, 8 and 9. The complete set of time dependent apparent R_d values for Co sorption onto biotite is given in Table A-3 in Appendix A.

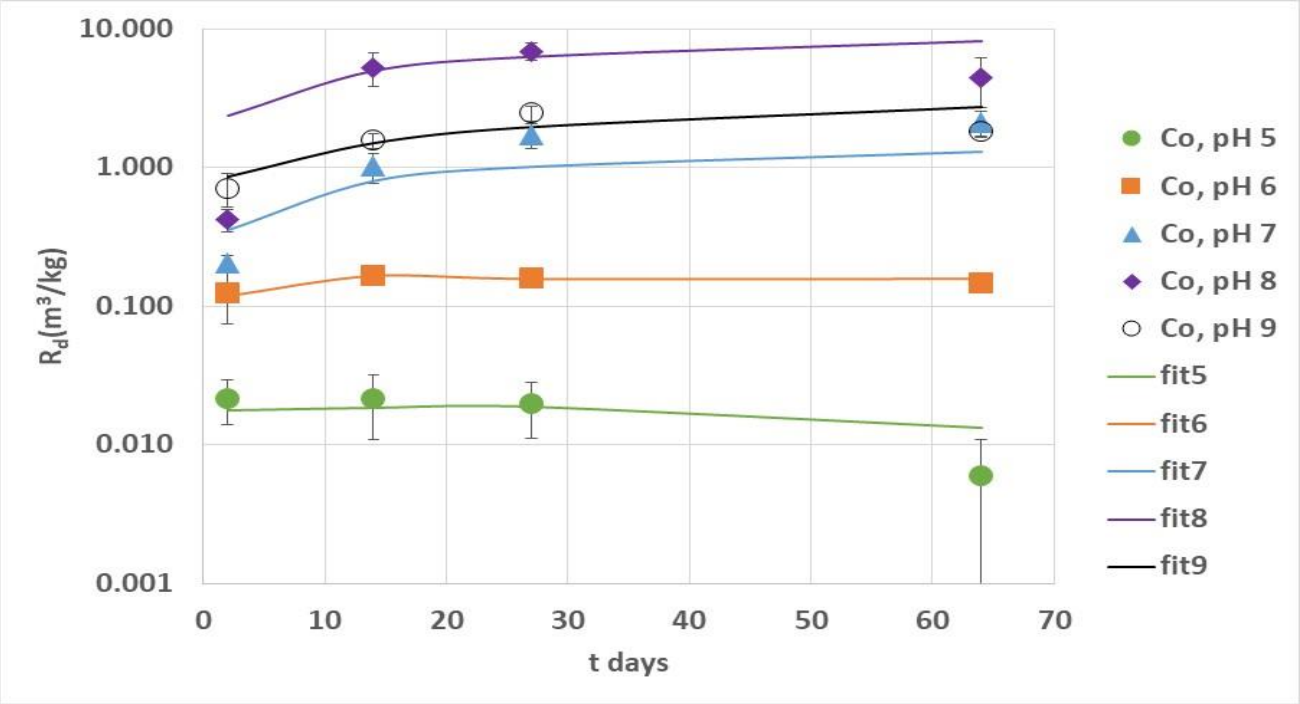

Figure 10. Measured R_d values for Co sorption onto biotite in 0.001 M $NaClO_4$ versus time.

The Co sorption onto biotite demonstrates a strong dependency on pH and, unlike Cs and Ba, the R_d values are more widely distributed with pH. A significant feature is also that Co sorption decreases from pH 8 to pH 9 (Fig.12), most likely due to the formation of hydroxide complexes of the Co^{2+} cation in solution.

Understanding the different forms of Co species in aqueous solutions is crucial for predicting its sorption onto biotite. In the pH range of 5 to 9, there are three distinct aqueous species of Co, namely $Co^{2+,}$ $Co(OH)^+$, and $Co(OH)_2$ where the di-hydroxide complex is the most stable, this is shown in Fig. 11.

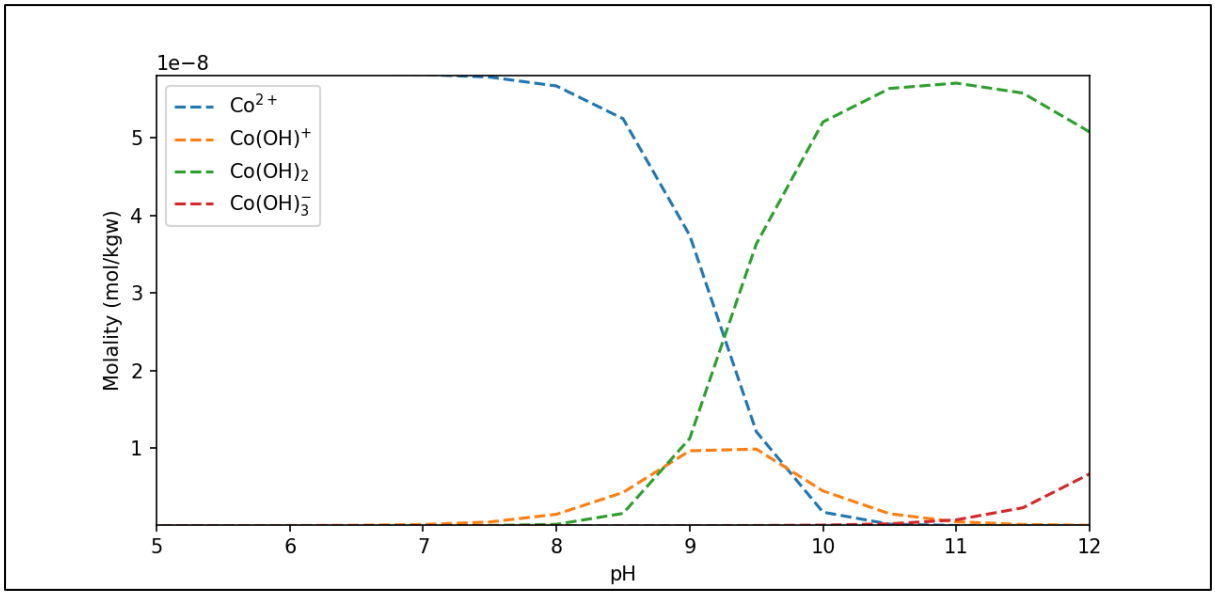

Figure 11. The speciation curve of Co (II) as a function of pH

Fig. 12 shows the data and fitting results for Co sorption on biotite as a function of pH and $NaClO_4$ concentration (0.001,0.01,0.1 M).

The amount of sorption increases within a narrow pH range of 6 to 8 but begins to decrease as the pH increases from 8 to 9 (Fig. 12). The sharp "edge" increase in sorption from pH 6 to 8 signifies that surface complexation, rather than ion exchange, is responsible for Co sorption [45]. In addition, when comparing of Co sorption data with respect to three different ionic strengths it suggests that there is virtually no effect of ionic strength on Co sorption which means that the metal is strongly bound to the surface, as reported by [46] in their study of ionic strength effects on cation sorption to oxides. This is further evidence for a surface complexation binding mechanism of Co to biotite.

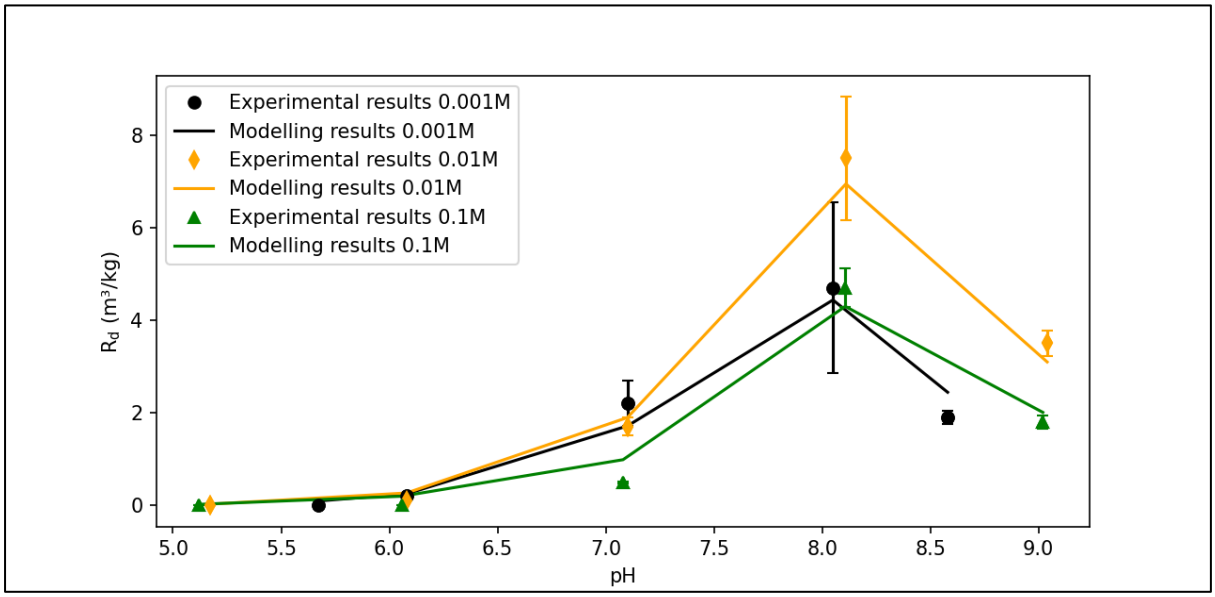

Figure 12. Co sorption on biotite in 0.001 M, 0.01 M, and 0.1 M $NaClO_4$ solutions.

It was found that only a surface complexation mechanism was needed to model the Co sorption onto biotite, this is shown for 0.001 M $NaClO_4$ in Fig 13. Figures for the other ionic strengths are available in Appendix B.

Three surface complexes ≡$SOCo^+$, ≡SOCoOH and ≡$SOCo(OH)_2^-$ were used to model the Co sorption data. Also, the "weak" complex ≡ $SOHCo^{2+}$ was initially included, but it was found to be insignificant for improving the fitting error and was therefore later excluded from model. For all ionic strengths, it was observed that the sorption on the biotite surface is mostly dominated by the ≡$SOCo^+$ and ≡SOCoOH surface complexes in the pH range that was investigated. A small contribution of ≡$SOCo(OH)_2^-$ was found for the highest pH. Table 6 shows the reactions and their constants.

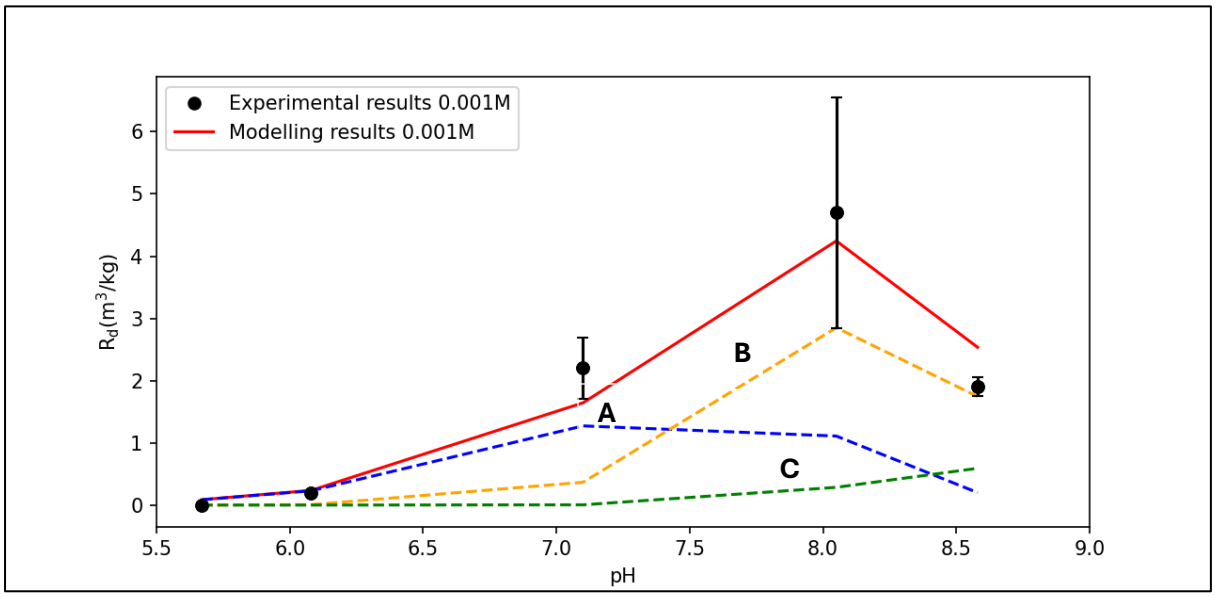

Figure 13. An example figure for Co sorption measurement (symbol) and modelling (continuous line) on biotite mineral in 0.001 M $NaClO_4$ solution. The contribution of different Co(II) species in its sorption is represented by different curves: (A: Blue line)≡$SOCo^+$; (B: yellow line)≡SOCoOH; (C: green line) ≡ $SOCo(OH)_2^-$.

Table 6: Modelled surface complexation and their associated constants at zero ionic strength (log_k°) for Co.

Reactions	**log k° (25 °C)**
≡ $SO^- + Co^{2+} \leftrightarrow \equiv SOCo^+$	5.4 ± 0.2
≡ $SO^- + Co(OH)^+ \leftrightarrow \equiv$ SOCoOH	7.3 ±0.5
≡ $SO^- + Co(OH)_2 \leftrightarrow \equiv SOCo(OH)_2^-$	4.8 ±0.3
≡ $SOH + Co^{2+} \leftrightarrow \equiv SOHCo^{2+}$	Not significant
$Co^{2+} + 2NaX \leftrightarrow CoX_2 + 2Na^+$	Not significant

*Inclusion of this species gave no improvement of error sum

3.3.4. Results for europium sorption onto biotite

The time-dependent results for Eu sorption onto biotite are shown in Fig.14, which shows that Eu sorption seems to stabilize after 30 days, although most data series show a slight increase up to 60 days. The complete set of time dependent apparent R_d values for Eu sorption onto biotite is given in Table A-4 in Appendix A.

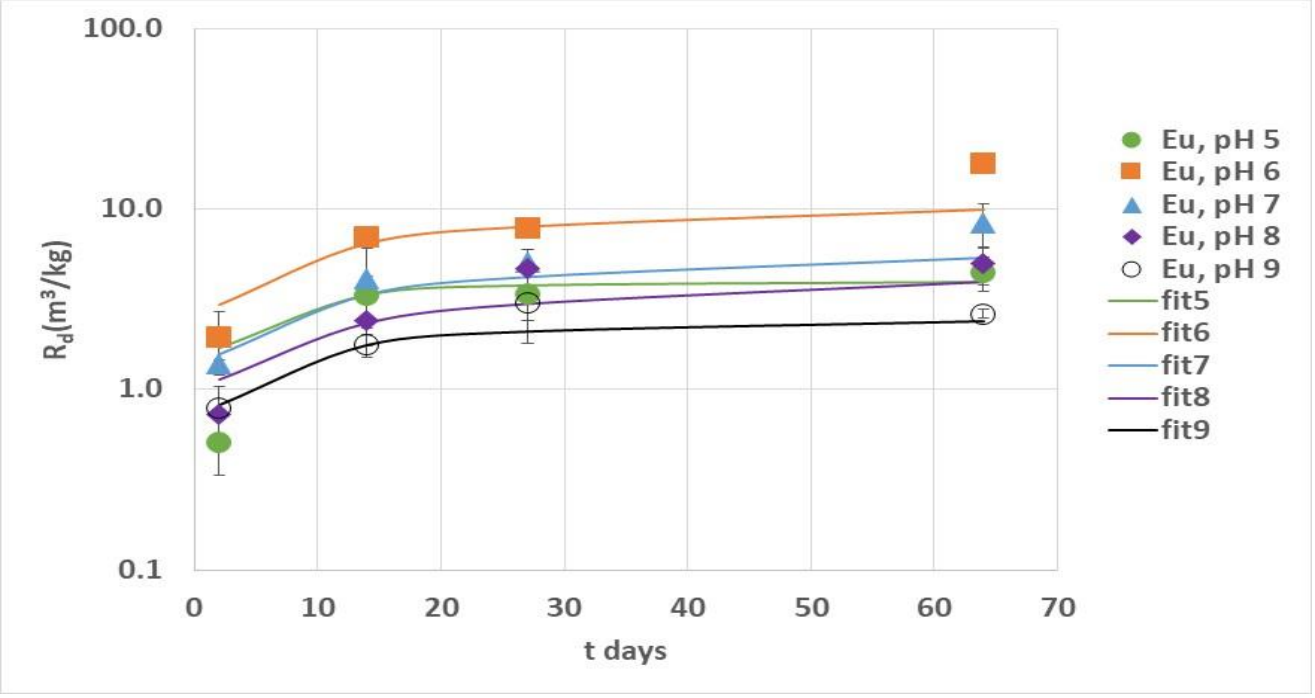

Figure 14. Measured R_d values for Eu sorption onto biotite in 0.001 M $NaClO_4$ versus time.

The last data point for pH 6 is unusually high but this is probably an effect of measuring close to detection limit: very few counts of ^{152}Eu were detected to obtain this value. Just as was found for Co, also Eu sorption becomes weaker at highest pH and, again, this is due to formation of the aqueous hydroxide complexes. A speciation of the different hydroxide complexes is shown in Fig.15.

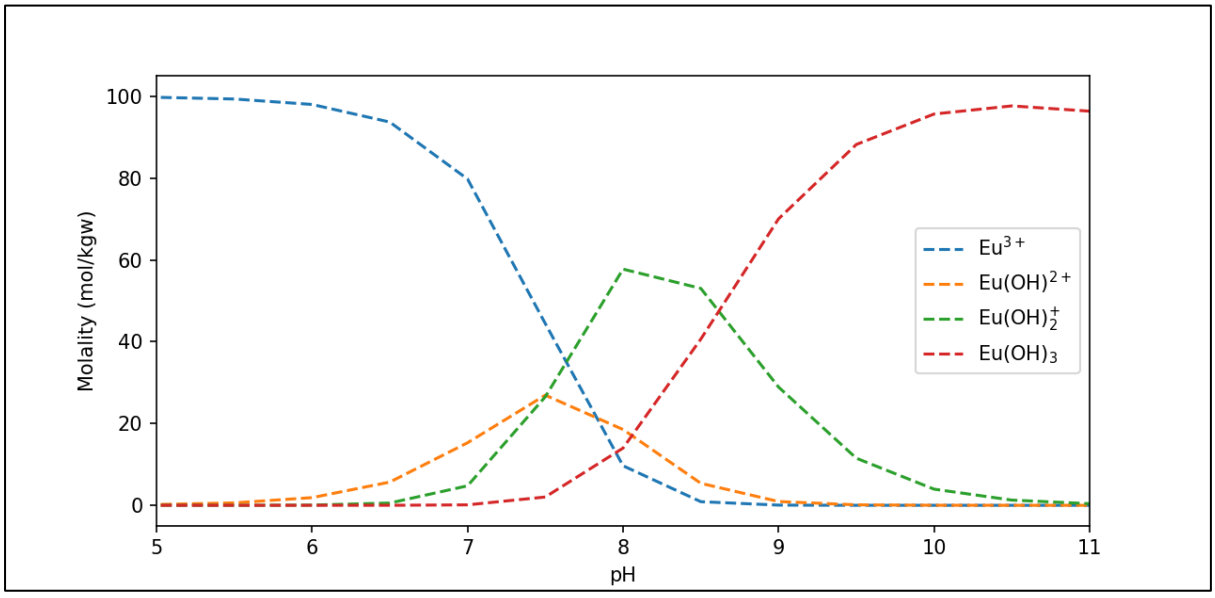

Figure 15. The aqueous speciation curve of Eu) as a function of pH

Fig. 15 shows that Eu, like Co, forms a variety of hydrolysis products in the pH range of 5 to 9. At a pH of lower then about 7.5, free Eu^{3+} is the dominant species. However, at a pH greater

than 7.5, the Eu^{3+} begins to form three hydrolysis products in sequence, namely $EuOH^{2+}$ $Eu(OH)_2^+$ and $Eu(OH)_3$.

The experimental and modeling results for Eu sorption onto biotite and three different $NaClO_4$ concentrations (0.001,0.01 and 0.1 M) are shown in Fig. 16.

The main findings were that at an ionic strength of 0.001 M, there was a significant increase in Eu sorption from pH ~5.5 to 6, followed by a gradual decrease up to pH 9, where the europium sorption again becomes very low. However, in the case of 0.01 and 0.1 M electrolytic solutions, the sorption edge appears to be more diffuse or even absent. The pH of maximum sorption has also increased to a higher pH value, although overall sorption is progressively lower the higher the ionic strength. The decrease in Eu sorption with pH above 7 can be attributed to its tendency to form hydroxyl species.

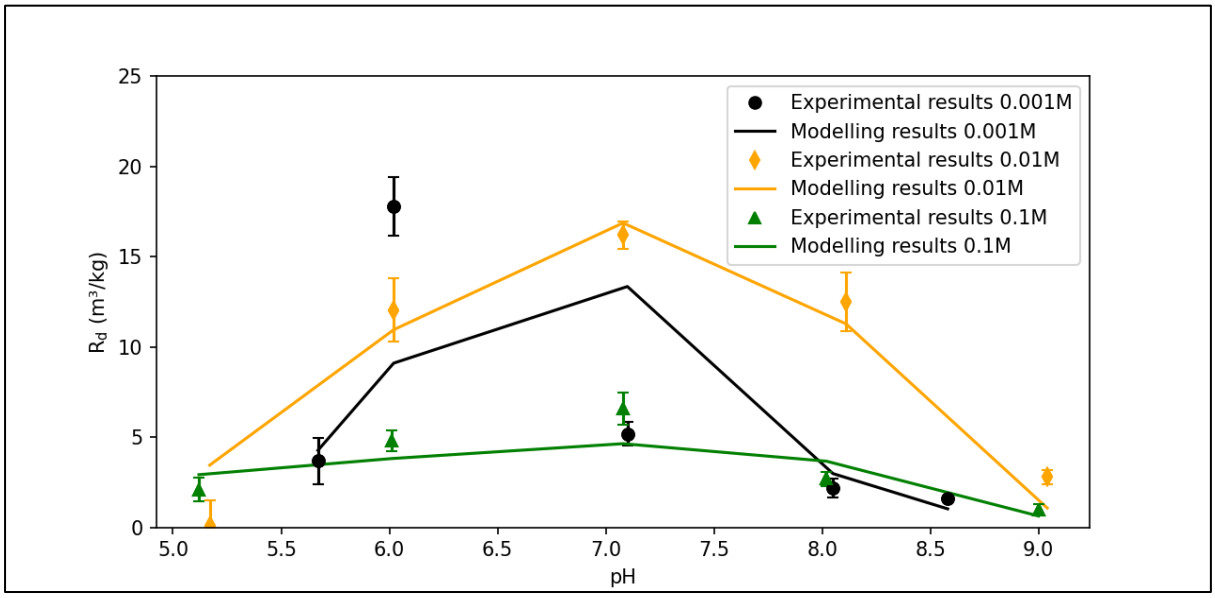

Figure 16. Eu sorption on biotite mineral in 0.001 M, 0.01 M, and 0.1 M $NaClO_4$ solutions.

Of the four metals investigated here, Eu shows the most complicated pattern of sorption and both surface complexation and cation exchange mechanisms were used to model the Eu sorption onto biotite. This is shown for 0.001 M $NaClO_4$ in Fig 17. Figures for the other ionic strengths are available in Appendix B.

The Eu sorption on biotite was modelled by considering three surface complexation species $\equiv SOEu^{2+}$, $\equiv SOEuOH^+$ and $\equiv SOEu(OH)_2$ and one exchange species EuX_3. Possible other surface species like $\equiv SOEu(OH)_3^-$ and $\equiv SOHEu^{3+}$ and their contributions to Eu sorption were considered but were found to be insignificant and was subsequently excluded from the model.

The model indicates that at pH ~ 6, the sorption is mainly dominated by an ion- exchange with the EuX_3 species. However, at a pH around 7, both the surface complexation species, $\equiv SOEu^{2+}$ and the ion-exchange species, EuX_3 are involved. At pH>8 the sorption is chiefly governed by surface complexation. The sorption "edge" that was found for Co at about pH 7 is evidently

present also for Eu, but it is diminished and sort of flattened out by the competition from cation exchange. This is decidedly different from what was found for Co, which showed no tendency to form surface exchange species.

Table 7 includes the reactions implemented as well as the related surface complexation and cation exchange constants.

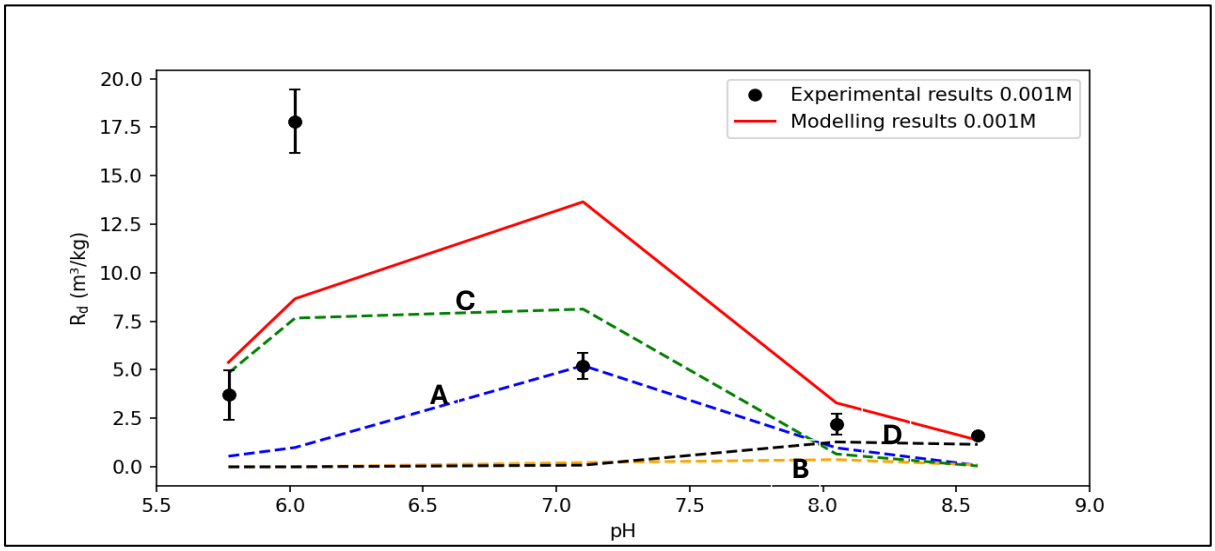

Figure 17. An example figure for Eu sorption measurement (symbol) and modelling (continuous line) on biotite mineral in 0.01 M NaClO4 solution. The contribution of different Eu(III) species in its sorption is represented by different curves: (A: blue line)≡ $SOEu^{2+}$; (B: yellow line) ≡ $SOEu(OH)^{+}$; (C: green line) EuX_3; (D: black line). ≡ $SOEu(OH)_2$

Table 7: Surface complexation and cation exchange reactions and their associated constants at zero ionic strength (log_k°) for Eu. Selectivity coefficients are for the specified ionic strength

Reactions	**log k° (25 °C)**
$\equiv SO^- + Eu^{3+} \leftrightarrow \equiv SOEu^{2+}$	6.2 ± 0.2
$\equiv SO^- + Eu(OH)^{2+} \leftrightarrow \equiv SOEu(OH)^{+}$	6.2 ± 0.9
$\equiv SO^- + Eu(OH)_2^{+} \leftrightarrow \equiv SOEu(OH)_2$	5.3 ± 0.3
$\equiv SOH + Eu^{3+} + 3H_2O \leftrightarrow \equiv SOEu(OH)_3^- + 4H^+$	Insignificant*
$\equiv SOH + Eu^{3+} \leftrightarrow \equiv SOHEu^{3+}$	Insignificant*

Reaction/Ionic Strength at 25 °C	0.001 M	0.01 M	0.1 M
$Eu^{3+} + 3NaX \leftrightarrow EuX3 + 3Na^+$	log_k = -2.6	log_k = 0.4	log_k = 3.3

*Inclusion of this species gave no improvement of error sum

3.3.5. Further discussion of results and comparisons with other studies

Typically, cation exchange is assumed to be independent of pH, but this appears not to be the case here. Figs. 5 shows that Cs sorption gradually decreases from pH 7 to 5 at all levels of background Na^+ concentration. This is probably an effect of H^+ competition for the exchange sites, also, surface complexation also starts to have an impact above pH 6. As already mentioned, literature data for Cs sorption on biotite at varying pH seems to be scarce [22]. Single values for Finnish biotite are reported with R_d=0.58m^3/kg at pH 6.9 and ~0.1 M NaCl by [47] and R_d=0.30m^3/kg at pH 9.7 and ~0.1 M NaX (X=mixed anions) by [17], however,

groundwater simulants were used in both these works. The SSA for the Finnish biotite was 1.4m^2/g, which gives R_a=0.42 and 0.22mm, respectively. In our work we found R_d=1.6m^3/kg at pH 7 and 0.001 M $NaClO_4$, which gives R_a=0.34mm, that is, a value in between those obtained by [47] and [17].

In this work, Ba show very similar sorption behaviour as Cs, although with the expected stronger attachment to the biotite due to increased charge of cation. Somewhat unexpectedly, however, is the involvement of aqueous $BaOH^+$ in sorption at high pH, according to model. Also similar with Cs, Fig. 8 shows that Ba sorption gradually decreases from pH 7 to 5 at all levels of background Na^+ concentration and surface complexation also start to have an impact above pH 6. Ba sorption on Finnish biotite at single fixed pH 8 and different ionic strengths have been studied by [21] and a picture shows R_d ~10 and 0.5m^3/kg for 0.01 and 0.1 M $NaClO_4$, respectively. SSA for their biotite was 0.64m^2/g, which gives R_a=16 and 0.8mm, respectively. In this work, at pH 8, we have got R_d=1.8 and 0.14m^3/kg for 0.01 and 0.1 M $NaClO_4$, respectively, which gives R_a=3.8 and 0.3mm, respectively, which are fairly comparable results to the literature values, although our results show a bit weaker Ba sorption on biotite than what was found by [21].

In this work, Co sorption onto biotite show a marked sorption "edge", starting at about pH 7 and maximizing at about pH 8 whereafter sorption decreases. The ionic strength had little influence on Co sorption. From a recent literature review, there seems to be no systematic sorption data for Co on biotite available, at least not in a wide range of conditions suitable for SCM purposes [22]. There is data for Ni reported in a wide pH range (3-9.5) and at two ionic strengths, 0.05 and 0.5M $NaClO_4$, by [25], which makes it suitable for comparison with the results here for Co. R_d values obtained for the lower ionic strength were about 0.1 M^3/kg in pH range 3-6, then a sorption "edge" starts rising the R_d values to a maximum of 20m^3/kg at pH 9.5. Interestingly, there were no drop in R_d values for Ni at this high pH value, also, the higher ionic strength had no effect on Ni sorption. A combination of one surface complex ($\equiv SONi^{1.5+}$) and one cation exchange species (NiX_2) were used to model Ni sorption, the latter was used for modelling sorption below the sorption "edge" (*ibid.*). The results are comparable to our results for Co, except that the decrease in sorption at highest pH for Co found here was not found for Ni [25]. Possibly, his can be explained by that a corresponding complex to the $Co(OH)_3^-$have not been proven to exist for Ni [48]

In the present study, Eu sorption onto biotite shows a somewhat complicated behaviour, with a sorption "edge" possibly overlaid by a substantial contribution from cation exchange. The result is an apparent change in pH for maximum sorption, depending on ionic strength. Eu sorption onto biotite at a wide range of conditions have also been studied by [25] and [15]. In the former work sorption at two different ionic strengths were investigated and it was found that Eu sorption was suppressed by high ionic strength at pH range 3-5. This is very similar to the results found here, but, more concerning, for the higher pH range the effect of ionic strength was not that obvious. The sorption was modelled with one surface complexation species $\equiv SOEu^{2+}$ and one exchange species EuX_3 [25]. However, since $[Eu]_{tot}$ was $9 \cdot 10^{-8}$M in the cited study, which is close by, or even over, the amorphous Eu hydroxide solubility limit [44], one

cannot exclude that a precipitation of $Eu(OH)_3$ (am) have taken place in the batch experiments, which may then show as apparent high, but erroneous, R_d values in the high pH range.

The second study mentioned found that the sorption edge already starts at pH 3, to reach a maximum (100% sorbed, R_d not reported) at pH 4 [15]. This seems to be too low in pH for the "edge" to appear, unless the biotite used have very different properties from the one used here. The separation was made with filtration, so one may suspect that filter sorption was measured and not biotite sorption. Similar effects on batch sorption results have been investigated and proved to be caused by filters for the phase separation [49].

In a follow up study to the present work, similar experiments were made at elevated temperatures (40 and 60°C). The results of evaluated enthalpy and entropy values for each surface reaction show that surface complexation and cation exchange reactions possess distinct signatures regarding these thermodynamic parameters. While surface complexation is driven by entropy, the cation exchange is driven by enthalpy [50].

5. Conclusions

The sorption of four cationic elements onto biotite mineral have been studied in the pH range 5-9, and the sorption of all elements show a considerable dependency on pH. This behavior was successfully modelled with a model which combines a 2-pKa surface complexation site, presumably on the biotite edges, and one cation exchange site, presumably on the basal planes.

Results show that both Cs and Ba sorption is decreased by competition from H+ and Na+ ions, which is explained by cation exchange as the main sorption mechanism, with Ba showing a tendency to also bind with surface complexation at high pH. Co, on the other hand, was found to bind to biotite by surface complexation only and any effect on its sorption by ionic strength was absent. Eu was found to have the most complicated sorption behavior of the elements investigated. A combination of surface complexation, including sorption of hydrolyzed species, and cation exchange were necessary to include in the modelling of Eu sorption onto biotite.

Implementation of sorption modelling was carried out successfully in several steps. These include in-diffusion model for time-dependency of apparent Rd values and the modelling of titration and batch sorption data with the use of PHREEQC geochemical modeling software in conjunction with an optimization routine written in PYTHON programming language. The results were a distinct set of effective diffusivities, surface complexation constants and cation selectivity coefficients for all metals.

6. Acknowledgment

This research was supported by grants from SSM (Swedish Radiation Safety Authority). We thank Dr. A.M. Jakobsson for her valuable comments, which helped us improve the manuscript.

Bibliography

[1] SKBF/KBS, “Kärnbränslecykelns slutsteg,” Svensk Kärnbränsleförsörjning AB (Swedish Nuclear Fuel and Waste Management Company), Stockholm, 1983.

[2] SKB, "Design and production of the KBS-3 repository (TR-10-12)," Svensk Kärnbränslehantering AB, Stockholm, 2010.

[3] A. Hedin and O. Olsson, "Crystalline rock as a repository for Swedish spent nuclear fuel," *Elements,* pp. 247-252, 2016.

[4] SKB, "Long-term safety for the final repository for spent nuclear fuel at Forsmark Main report of the SR-Site project Volume III (TR-11-01)," Svensk Kärnbränslehantering AB, Stockholm, 2011.

[5] B. Miller and N. Marcos, "Process report - FEPs and scenarios for a spent fuel repository at Olkiluoto (Posiva Report 2007-12)," Posiva Oy, Olkiluoto, Finland, 2007.

[6] J. Crawford, "Bedrock Kd data and uncertainty assessment for application in SR-Site geosphere transport calculations (R-10-48)," Svensk Kärnbränslehantering AB, Stockholm, 2010.

[7] M. Hakanen, H. Ervanne and E. Puukko, "Safety case for the disposal of spent nuclear fuel at Olkiluoto - Radionuclide migration parameters for the geosphere (2012-41)," Posiva Oy, Olkiluoto, Finland, 2012.

[8] J. A. Davis, J. A. Coston, D. B. Kent and C. C. Fuller, "Application of the surface complexation concept to complex mineral assemblages," *Env. Sci. Technol.,* vol. 32, pp. 2820-2828, 1998.

[9] J. A. Davis, D. E. Meece, M. Kohler and G. P. Curtis, "Approaches to surface complexation modeling of uranium(VI) adsorption on aquifier sediments," *Geochim. Cosmochim. Acta,* vol. 68, pp. 3261-3641, 2004.

[10] H. Drake, B. Sandström and E.-L. Tullborg, "Mineralogy and geochemistry of rocks and fracture fillings from Forsmark and Oskarshamn: Compilation of data for SR-Can (R-06-109)," Svensk Kärnbränslehantering AB, Stockholm, 2006.

[11] E. Selnert, J. Byegård and H. Widestrand, "Forsmark site investigation - Laboratory measurements within the site investigation programme for the transprt properties of the rock, Final report (P-07-139)," Svensk Kärnbränslehantering AB, Stockholm, 2008.

[12] W. D. Nesse, Introduction to mineralogy, New York: Oxford University Press, 2000.

[13] R. M. Cornell, "Adsorption of cesium on minerals: A review," *J Radioanal. Nucl. Chem.,* vol. 171, pp. 483-500, 1993.

[14] S.-C. Tsai, T.-H. Wang, M.-H. Li, Y.-Y. Wei and S.-P. Teng, "Cesium adsorption and distribution onto crushed granite under different physicochemical conditions," *J. Hazard. Mat.,* vol. 161, pp. 854-861, 2009.

[15] K. Fukushi, Y. Hasegawa, K. Maeda, Y. Aoi, A. Tamura, S. Arai, Y. Yamamoto, D. Aosai and T. Mizuno, "Sorption of Eu(III) on granite: EPMA, LA-ICP-MS, batch and modeling studies," *Environ. Sci. Technol.,* vol. 47, pp. 12811-12818, 2013.

[16] Y. Tachi, T. Ebina, C. Takeda, T. Saito, H. Takahashi, Y. Ohuchi and A. J. Martin, "Matrix diffusion and sorption of Cs, Na, I and HTO in granodiorite: Laboratory-scale results and their extrapolation to the in situ conditions," *J. Contam. Hydrol.,* vol. 179, pp. 10-24, 2015.

[17] E. Muuri, J. Ikonen, M. Matara-aho, A. Lindberg, S. Holgersson, M. Voutilainen, M. Siitari-Kauppi and A. Martin, "Bahavior of Cs in Grimsel granodiorite: sorption on main minerals and crushed rock," *Radiochim. Acta,* vol. 104, pp. 575-582, 2016.

[18] K. L. Nagy, "Dissolution and precipitation kinetics of sheet silicates," *Rev. Mineral.,* vol. 31, pp. 173-225, 1995.

[19] J. P. McKinley, J. M. Zachara, S. M. Heald, A. Dohnalkova, M. G. Newville and S. R. Sutton, "Microscale distribution of cesium sorbed to Bbiotite and muscovite," *Environ. Sci. Technol.,* vol. 38, pp. 1017-1023, 2004.

[20] J. Kyllönen, M. Hakanen, A. Lindberg, R. Harjula, M. Vehkamäki and J. Lehto, "Modeling of cesium sorption on biotite using cation exchange selectivity coefficients," *Radiochim. Acta,* vol. 102, pp. 919-929, 2014.

[21] M. Söderlund, H. Ervänne, E. Muuri and J. Lehto, "The sorption of alkaline earth metals on biotite," *Geochem. J.,* vol. 53, pp. 223-234, 2019.

[22] S. Holgersson and P. Kumar, "A literature review on thermodynamic sorption models of radionuclides with some selected granitic minerals," *Front. Nucl. Eng.,* p. 1227170, 2023.

[23] T. E. Payne, V. Brendler, M. Ochs, B. Baeyens, P. L. Brown, J. A. Davis, C. Ekberg, D. A. Kulik, J. Luetzenkirchen, T. Missana, Y. Tachi, L. R. Van Loon and S. Altmann, "Guidelines for thermodynamic sorption modelling in the context of radioactive waste disposal," *Environ. Modell. Softw.,* vol. 42, pp. 143-156, 2013.

[24] X. Li, E. Puhakka, L. Liu, W. Zhang, J. Ikonen, A. Lindberg and M. Siitari-Kauppi, "Multi-site surface complexation modelling of Se(IV) sorption on biotite," *Chem. Geol.,* vol. 533, 2020.

[25] E. Puukko, M. Olin, E. Puhakka, M. Hakanen, A. Lindberg and J. Lehikoinen, "Sorption of nickel and europium on biotite," *In FUNMIG 3rd Annual Meeting,* pp. 265-272, 2007.

[26] S. Holgersson, H. Drake, A. Karlsson and L. Krall, "Biotite dissolution kinetics at pH 4 and 6.5 under anaerobic conditions and the release of dissolved Fe(II)," *Chem.Geol.,* vol. 662, p. 122204, 2024.

[27] I. Dubois, *Specific surface area of some minerals commonly found in granite,* Stockholm: Kungliga Tekniska Högskolan, 2011.

[28] S. Brunauer, P. H. Emmet and E. Teller, “Adsorption of gases in multimolecular layers,” *J. Am. Chem. Soc.,* vol. 60, pp. 309-319, 1938.

[29] C. Schollenberger and R. Simon, "Determination of exchange capacity and exchangeable bases in soil—ammonium acetate method," *Soil Sci.,* vol. 59, pp. 13-24, 1945.

[30] Y. G. Berubé, G. Y. Onoda and P. L. De Bruyn, "Proton adsorption at the ferric oxide/aqueous solution interface," *Surface Science,* vol. 8, pp. 448-461, 1967.

[31] G. Gran, "Determination of the equivalent point in potentiometric titrations," *Acta Chem. Scand.,* vol. 4, pp. 557-559, 1950.

[32] A. Jakobsson, Y. Albinsson and R. Rundberg, "Studies of surface complexation of H+ , NpO2+, Co2+, Th4+ onto TiO2 and H+, UO22+ onto alumina (TR-98-15)," Svensk Kärnbränslehantering AB, Stockholm, 1998.

[33] Å. Zazzi, A. Jakobsson and S. Wold, "Ni (II) sorption on natural chlorite," *Appl. Geochem.,* vol. 27, pp. 1189-1193, 2012.

[34] A. W. Bray, L. G. Benning, S. Bonneville and E. H. Oelkers, "Biotite surface chemistry as a function of aqueous fluid composition," *Geochi. Cosmochim. Acta,* vol. 128, pp. 58-70, 2014.

[35] Q. Yu, A. Kandegedara, Y. Xu and D. B. Rorabacher, “Avoiding interferences from Good´s buffers: a contiuous series of noncomplexing tertiary amine buffers covering the entire range of pH 3-11,” *Anal. Biochem.,* vol. 253, pp. 50-56, 1997.

[36] M. Andersson, H. Ervanne, M. A. Glaus, S. Holgersson, P. Karttunen, H. Laine, B. Lothenbach, I. Puigdomenech, B. Schwyn, M. Snellman, H. Ueda, M. Vuorio, E. Wieland and T. Yamamoto, "Development of methodology for evaluation of long-term safety aspects of organic cement paste components Working Report 2008-28," Posiva Oy, Olkiluoto, Finland, 2008.

[37] J. Crank, The Mathematics of diffusion, 2nd ed., New York: Oxford University Press, 1979.

[38] A. W. Bray, E. H. Oelkers, S. Bonneville, D. Wolff-Boenisch, N. J. Potts, G. Fones and L. G. Benning, "The effect of pH, grain size and organic ligands on biotite weathering rates," *Geochimica et Cosmochimica Acta,* vol. 164, pp. 127-145, 2015.

[39] M. Kosmulski, "The pH dependent surface charging and points of zero charge. VIII Update.," *Adv.Colloid Interface Sc.,* p. 102064, 2020.

[40] F. Macht, K. Eusterhues, G. J. Pronk and K. U. Totsche, "Specific surface area of clay minerals: Comparison between atomic force microscopy meaurements and bulk.gas (N2) and -liquid (EGME) adsorption methods," *App. Clay. Sci.,* pp. 20-26, 2011.

[41] D. L. Parkhurst and C. A. J. Appelo, *PHREEQC version 3: Computer Program for Speciation, Batch-Reaction, One-Dimensional Transport, and Inverse Geochemical Calculations,* U.S. Geological Survey, 2021.

[42] S. R. Charlton and D. L. Parkhurst, "Modules based on the geochemical model PHREEQC for use in scripting and programming languages," *Comput. Geosci.,* vol. 37, pp. 1653-1663, 2011.

[43] L. Wissmeier and D. A. Barry, "Simulation tool for variably saturated flow with comprehensive geochemical raction in the two and three dimensional domains," *Env. Modell. Softw.,* vol. 26, pp. 210-218, 2011.

[44] N. Jordan, T. Thoenen, K. Spahiu, J. Kelling, S. Starke and V. Brendler, "A critical review of the solution chemistry, solubility, and thermodynamics of europium: Recent advances on the Eu(III) hydrolysis," *Coordin. Chem. Rev.,* vol. 510, p. 215702, 2024.

[45] W. Stumm and J. J. Morgan, Aquatic Chemistry, 3rd Ed., New York: Wiley, 1996.

[46] J. Luetzenkirchen, "Ionic strength effects on cation sorption to oxides: Macroscopic observations and their significance in microscopic interpretation," *J. Colloid. Interface Sci.,* vol. 195, pp. 149-155, 1997.

[47] E. Muuri, M. Siitari-Kauppi, M. Matara-aho, J. Ikonen, A. Lindberg, L. Qian and L. Koskinen, "Cesium sorption and diffusion on crystalline rock: Olkiluoto casestudy," *Journal of Radioanalytical and Nuclear Chemistry,* vol. 311, pp. 439-446, 2017.

[48] C. Ekberg and P. L. Brown, Hydrolysis of metal ions. Vol. 1 and 2., Wiley-VCH, 2016.

[49] S. Holgersson, "Studies on batch sorption methodologies: Eu sorption onto Kivetty granite," *Procedia Chemistry,* vol. 7, pp. 629-640, 2012.

[50] P. Kumar, S. Holgersson and C. Ekberg, "Sorption of Cs, Ba, Co and Eu onto biotite at 40 and 60 C - a combined experimental and modelling study," *J. Contamin. Hydrol.,* in press.